Free-stream Turbulence Effects on Vortex Shedding: A CFD Study

A Thesis

submitted to
Indian Institute of Science Education and Research Pune
in partial fulfilment of the requirements for the
BS-MS Dual Degree Programme

by

Rohan Hela

Indian Institute of Science Education and Research Pune
Dr. Homi Bhabha Road,
Pashan, Pune 411008, India.

April, 2024

Supervisor: Dr. Vagesh D. Narasimhamurthy

Certificate

This is to certify that this dissertation entitled Free-stream Turbulence Effects on Vortex Shedding: A CFD Study towards the partial fulfilment of the BS-MS dual degree programme at the Indian Institute of Science Education and Research, Pune represents study/work carried out by Rohan Hela at Indian Institute of Technology, Madras under the supervision of Dr. Vagesh D. Narasimhamurthy, Professor, Department of Applied Mechanics & Biomedical Engineering , during the academic year 2019-2024.

Dr. Vagesh D. Narasimhamurthy

Committee:

Dr. Vagesh D. Narasimhamurthy

Dr. Prasad Subramanian

This thesis is dedicated to my parents

Declaration

I hereby declare that the matter embodied in the report entitled Free-stream Turbulence Effects on Vortex Shedding: A CFD Study are the results of the work carried out by me at the Department of Applied Mechanics & Biomedical Engineering, Indian Institute of Technology, Madras, under the supervision of Dr. Vagesh D. Narasimhamurthy and the same has not been submitted elsewhere for any other degree. Wherever others contribute, every effort is made to indicate this clearly, with due reference to the literature and acknowledgement of collaborative research and discussions.

Rohan

Rohan Hela

Acknowledgments

I am sincerely grateful to my supervisor, Dr. Vagesh D. Narasimhamurthy, for entrusting me with this incredible opportunity, as well as for his excellent supervision, constant support, and essential insights throughout this research project. Without his mentorship, compassion, and assistance, this task would not have been completed.

I am grateful to the members of the laboratory where this research was conducted. Their collaborative spirit, insightful discussions, and gracious support greatly improved the quality and depth of this research.

I would like to thank Dr. Prasad Subramanian, for being a part of my TAC and for his handling of the academic processes involved, which aided the smooth progress of this project.

I am genuinely grateful to my friends and family for their consistent support, understanding, and belief in my abilities. Throughout this journey, their support has provided tremendous strength and drive.

I extend my heartfelt appreciation and gratitude to everyone mentioned above, as well as countless more, who have helped me improve personally and academically.

Contents

List of Figures

List of Tables

Nomenclature

Greek Symbols

ρ	density
μ	dynamic viscosity
Δ	grid spacing or filter width
Re	Reynolds number
θ	polar angle from the stagnation point
k	wavenumber
$\hat{u}_k$	Fourier coefficient
θ_k	phase
σ	integral length scale
ω'	vorticity
ν_t	eddy viscosity

Roman Symbols

St	Strouhal number
f	shedding frequency
L	characteristic length
U_∞	flow velocity
u_i	tensor notation for velocity components: $u_1 = u, u_2 = v, u_3 = w$
x_i	tensor notation for spatial coordinates: $x_1 = x, x_2 = y, x_3 = z$
τ_{ij}	stress tensor
t	time
p	hydrostatic pressure

$\mathbf{U}$	mean velocity
$\mathbf{u}$	velocity fluctuation
δ_{ij}	Kronecker delta
S_{ij}	strain tensor
$\bar{\phi}$	spatial filtered function
ϕ	unfiltered function
ϕ'	fluctuating component
u, v, w	stream-wise, cross-stream and spanwise velocity component
d	diameter
C_p	pressure coefficient
p_{ref}	spatially averaged pressure
$E(\lvert k \rvert)$	energy spectrum
u'	synthesized velocity field
x^k	eddy position, 3-component vector: (x_1^k, x_2^k, x_3^k)
α^k	eddy intensity, 3-component vector: $(\alpha_1^k, \alpha_2^k, \alpha_3^k)$
S	set of points
a_{ij}	Lund coefficient - Cholesky decomposition of the Reynolds stress tensor
$f_{\sigma(\mathbf{x})}$	shape function
c_k	eddy amplitude
V_B	volume of eddy box
R_{ij}	Reynolds stress component
U_b	bulk velocity
$\mathbf{r}_k$	distance between a point and an eddy
d_k	module of r_k
l_{LES}	LES length scale

Acronyms

CFD	Computational Fluid-Dynamic
LES	Large Eddy Simulation
SGS	Sub-Grid Scales
DNS	Direct Numerical Solution
RANS	Reynolds Averaged Navier Stokes
SEM	Synthetic Eddy Method

DFSEM	Divergence Free SEM
FVM	Finite Volume Method
HIT	Homogeneous Isotropic Turbulence
FST	Free-Stream Turbulence
SRFM	Synthetic Random Fourier Method
SDFM	Synthetic Digital Filtering Method
SVFM	Synthetic Volume Forcing Method

Abstract

This study investigates the nuances of the effects of free-stream turbulence (FST) on bluff bodies using a method that blends computational fluid dynamics (CFD) simulations and synthetic turbulence generation techniques.

This research focuses on using the divergence-free synthetic eddy method (DFSEM), a synthetic turbulence generator for the inlet condition, for large eddy simulation (LES) using OpenFOAM. This open-source CFD solver leverages the finite volume method (FVM). DFSEM mimics the structural properties of turbulence by carefully injecting randomly generated eddies into the velocity field, resulting in turbulence-like fluctuations. The parameters of the approach, such as mean velocity, integral length scale, and Reynolds stress, are critical in determining turbulent flow properties. The flow is treated as homogeneous isotropic turbulence (HIT), and the turbulence intensity is assumed to be 10%.

The simulations in this work are focused on bluff bodies, particularly cylinders and spheres, to evaluate the effect of free-stream turbulence (FST) on their aerodynamic properties. The study investigates how synthetic turbulence affects the vortex-shedding phenomenon around these bluff bodies. The findings emphasize the complex interplay between free-stream turbulence and bluff body aerodynamics, providing essential insights into flow behaviour and shedding light on fundamental features of turbulent flow dynamics.

The study's significance goes beyond fundamental research, with potential applications ranging from sports aerodynamics, particularly in tennis, where seam structure is critical, to advances in LES techniques. By explaining the complex interaction between free-stream turbulence and bluff body aerodynamics within the LES framework, this study sets the way for future research into turbulence modelling and aerodynamic optimization, providing significant insights into real-world flow phenomena.

Chapter 1

Introduction

The study of turbulence is one of the most fascinating phenomena in physics. The primary definition of turbulence is chaotic flow that exhibits specific statistical patterns or structures. It is crucial in several engineering fields, like combustion and aeronautics.

The study of bluff body flows is a classical yet highly complex subject in turbulence and fluid dynamics. In contrast to streamlined bodies like airfoils, bluff body flow is the fluid motion surrounding a solid object with a blunt or rounded shape.

The geometry of bluff bodies, such as cylinders, spheres, and flat plates, interacts with the incoming flow to produce complicated flow patterns. Large-scale vortices are formed when the fluid separates from the body's surface at moderate to high Reynolds numbers. These flows usually show separation areas. These vortices aid in forming a wake region characterized by varying flow velocities and low-pressure areas downstream of the body.

Aeronautics, civil engineering, automotive design, and other engineering fields all place a high priority on understanding bluff body flows. Applications include lowering drag in industrial operations, improving heat exchanger efficiency, and optimizing vehicle aerodynamics. In addition, bluff body flows are primary test cases for theoretical models and computational fluid dynamics (CFD) simulations used to clarify the intricacies of turbulent processes.

1.1 Objective

The aims of this project are as follows:

- To study the phenomenon of vortex shedding on different canonical objects like cylinders, spheres, etc., computationally and validate with experimental results.

- Apply free-stream turbulence on the incoming flow and investigate the resulting vortex shedding.

1.2 Thesis outline

The thesis has five sections: The theoretical and methodological foundation for fluid dynamics, turbulence theory, and numerical simulation techniques are laid out in Chapter 2. As a tutorial test case, Chapter 3 provides a detailed methodology on how to set up and run a flow physics simulation. In Chapter 4, different approaches in fluid dynamics research are examined through a survey of the literature on synthetic turbulence techniques. In chapter 5, synthetic turbulence is finally implemented using numerical simulations. In Chapter 6, our findings will be summarized, and conclusive remarks will be provided. The approach is described, and the results are analyzed to comprehend the effect of turbulence on flow behaviour.

Chapter 2

Theoretical and Computational Background

This chapter will cover key theoretical and methodological knowledge crucial to the investigation. It will be divided into two sections that will explain the governing equations as well as the numerical techniques that are critical to understanding the research.

2.1 Introduction

Bluff body flows are the central focus of this study, often characterized by the generation of vortices. This phenomenon happens when the stable vortex pairs undergo a temporal transition beyond a certain critical Reynolds number (Re). An adverse pressure gradient causes flow separation, which results in the creation of shear layers and a significant rise in vorticity. It results in shear generating a layer that rolls into a vortex, which occurs with a specific vortex shedding frequency (f). That is determined by the Reynolds number. The 'Strouhal number'(St) of the normalized vortex shedding frequency is recognized as,

$$St = f \cdot \frac{L}{U_\infty}$$

where L is the characteristic length (for example, diameter of sphere or cylinder or aerofoil thickness) and U_∞ is the flow velocity.

2.2 Governing equations

Fluid dynamics can be described using a set of equations, each describing a specific aspect of it, such as:

- mass conservation → Continuity equation

$$\frac{D\rho}{Dt} + \rho \cdot \frac{\partial u_i}{\partial x_i} = 0 \tag{2.1}$$

where $\frac{D\rho}{Dt}$ is known as the material derivative, and is written as,

$$\frac{\partial \rho}{\partial t} + u_i \cdot \frac{\partial \rho}{\partial x_i} = 0 \tag{2.2}$$

- momentum conservation → Momentum equation

$$\frac{\partial(\rho u_j)}{\partial t} + \frac{\partial(\rho u_i u_j)}{\partial x_i} = \rho g_j + \frac{\partial \tau_{ij}}{\partial x_i} \tag{2.3}$$

Within the framework of this study, the simulation of situations involving incompressible flow is the exclusive focus. This involves the presumption that basic characteristics like the mass density, represented by ρ, and the dynamic viscosity, represented by μ, stay constant across the flow domain. Moreover, gravitational effects are deemed insignificant for the purposes of this study and are therefore not taken into consideration.

Thus, the continuity equation is given as,

$$\frac{\partial u_j}{\partial x_j} = 0 \tag{2.4}$$

And the momentum equation becomes,

$$\rho \frac{Du_i}{Dt} = \frac{\partial \tau_{ij}}{\partial x_j} \tag{2.5}$$

2.2.1 Newtonian fluid

When dealing with a Newtonian fluid, the stress-strain relationship simplifies considerably, facilitating a more straightforward approach to the equations. The continuity equation (equation 2.4) has three unknown parameters and the momentum equation (equation 2.5) has three unknown parameter for each set of three equations, thus resulting in total of twelve unknown parameter with four equations, indeed making the direct solution impractical. To address this, a constitutive relation is employed, which helps in the closure of the set of the above two equations by making a constitutive relation between the stress tensor τ_{ij} and the velocity gradient tensor $u_i x_j$, which is given by

$$\tau_{ij} = -p\delta_{ij} + 2\mu S_{ij} \tag{2.6}$$

Where τ_{ij} is the stress tensor, p is the hydrostatic pressure, δ_{ij} is the Kronecker delta, μ is the dynamic viscosity, and S_{ij} is the strain tensor.

2.2.2 Navier Stokes equation

Upon substitution of Equation 2.6 into Equation 2.5, the resultant equation becomes:

$$\rho \frac{Du_i}{Dt} = -\frac{\partial p}{\partial x_i} + \mu \frac{\partial^2 u_i}{\partial x_j^2} \tag{2.7}$$

This equation represents the conservation of momentum for an incompressible Newtonian fluid. It signifies the balance between the rate of change of momentum, pressure gradients, and viscous forces.

Collectively, Equation 2.7 and Equation 2.4 forms the Navier-Stokes equations, which provides a comprehensive description of fluids. With four equations and four unknowns, these equations can be solved to determine the flow characteristics fully.

2.3 Numerical schemes

This study is performed using the open-source CFD solver, known as OpenFOAM (Open Field Operation and Manipulation).

2.3.1 CFD working principle

Numerical methods and data analysis are used to solve and understand problems relating to fluid flow. The analysis process for CFD starts with a mathematical model of the underlying physical problem. All areas of the region of interest must satisfy the conservation laws of mass, momentum, and energy. Setting the proper initial and boundary conditions is the prerequisite for solving the problem.

To simulate fluid flow and related processes, the solver uses the finite volume method (FVM), and it divides the domain of the solution into a finite number of control volumes (CV) and applies the conservation equations to every CV. In this stage, the differential equation is discretized, transformed into algebraic equations, and iteratively solved. The collective term for the cells is the grid.

At each node or cell center, the set of algebraic equations—which represent the discretized form of the differential equation—is numerically solved (on a computer) for the flow field variables. The solution to a system of equations is obtained numerically. To get to a converged solution, several iterations are typically required. When there are minimal changes (less than the tolerance value set) in the solution variables between iterations, convergence is achieved.

The validity of a convergent solution depends on the applicability and correctness of the physical models, problem formulation, and grid resolution. To extract quantities of interest (such as lift, drag, torque, heat transfer, separation, pressure loss, etc.), the solution is then post-processed.

2.3.2 Large Eddy Simulation (LES)

In direct numerical simulation (DNS), the Navier-Stokes equations are simulated without modelling turbulence, resolving all scales of motion accurately through the numerical grid. The primary source of error in DNS comes from the numerical method itself. However, it is computationally expensive because DNS must mimic an extensive range of scales.

To tackle this problem, large eddy simulation (LES) uses a turbulence model to capture the impacts of lower scales while directly simulating the larger scales of turbulence. This method preserves the key characteristics of turbulent flow while drastically cutting computing costs compared to DNS. The Kolmogorov theory provides support for LES modelling, arguing that tiny scales in the inertial and dissipative range exhibit universal behaviour and may be parameterized by the energy transfer rate entering the cascade alone [1].

In the case of managing lower length scales, LES employs a set of filtering equations aiming to address the more significant turbulence length scales containing energy. The spatial filtering operation is defined by a filter function $G(x,x',\Delta)$ given as [2]:

$$\bar{\phi}(x,t) = \int_{-\infty}^{\infty}\int_{-\infty}^{\infty}\int_{-\infty}^{\infty} G(x,x',\Delta)\phi(x',t)\,dx'_1\,dx'_2\,dx'_3 \tag{2.8}$$

where Δ is the filter cutoff width, $\phi(x,t)$ is the unfiltered function, and $\bar{\phi}(x,t)$ is the filtered function. Over-bar here represents spatial filtering rather than time-averaging. Also, it can be further written as:

$$\bar{\phi} = \phi + \phi' \tag{2.9}$$

Numerous filtering functions G can be employed, such as top-hat, Gaussian, and spectral cutoff defined by Laborasse and Sagaut. [3] . The filtered Navier-Stokes equation are:

Continuity

$$\frac{\partial(\rho\bar{u}_i)}{\partial x_i} = 0 \tag{2.10}$$

Momentum

$$\rho\frac{\partial \bar{u}_i}{\partial t} + \rho\frac{\partial \bar{u}_i\bar{u}_j}{\partial x_i} = -\frac{\partial \bar{p}}{\partial x_i} + \frac{\partial}{\partial x_j}\left(\mu\left(\frac{\partial \bar{u}_i}{\partial x_j} + \frac{\partial \bar{u}_j}{\partial x_i}\right)\right) - \rho\frac{\partial}{\partial x_j}(\overline{u_i u_j} - \bar{u}_i\bar{u}_j) \tag{2.11}$$

The residual-stress tensor in the momentum filtered equation is given as,

$$\tau_{ij} = \rho\overline{u_i u_j} - \rho\bar{u}_i\bar{u}_j. \tag{2.12}$$

from equation equation 2.9, $\overline{u_i u_j} = \overline{\bar{u}_i\bar{u}_j} + \overline{u'_i\bar{u}_j} + \overline{\bar{u}_i u'_j} + \overline{u'_i u'_j}$. Putting this in equation 2.12, it becomes,

$$\tau_{ij} = (\rho\overline{\bar{u}_i\bar{u}_j} - \rho\bar{u}_i\bar{u}_j) + (\rho\overline{u'_i\bar{u}_j} + \rho\overline{\bar{u}_i u'_j}) + \rho\overline{u'_i u'_j} \tag{2.13}$$

Each terms in the equation 2.13 are sub-grid scales (SGS) stress contributions [4], which are :

1. Leonard stresses $L_{ij} = \rho(\overline{\bar{u}_i\bar{u}_j} - \bar{u}_i\bar{u}_j)$
2. Cross-stresses $C_{ij} = \rho(\overline{u'_i\bar{u}_j} + \overline{\bar{u}_i u'_j} - \bar{\bar{u}}_i\bar{u}'_j - \bar{u}'_i\bar{\bar{u}}_j)$
3. SGS Reynolds stresses $R_{ij} = \rho(\overline{u'_i u'_j} - \bar{u}_i\bar{u}_j)$

The effects at the resolved scales are the Leonard stresses L_{ij}. The interaction between the resolved flow and the SGS eddies is responsible for the cross-stresses C_{ij}. And SGS turbulence model is utilized to simulate the LES Reynolds stresses R_{ij}, which are brought on by convective momentum transfer resulting from interactions of SGS eddies. Two of the SGS models are discussed in chapter 5.

2.3.3 OpenFOAM and its implementation

OpenFOAM is an open-source CFD solver. Given its modular arrangement, users can expand and modify the code to meet their unique requirements and research goals. Additionally, the solver has undergone comprehensive validation and verification against benchmark cases and experimental data, giving users confidence in its dependability and accuracy for research applications. The time discretization scheme used was second-order implicit. The spatial derivative was discretized using first-order central differences approximations. The convective flux on the cell surface was estimated by blending the central differences with 25% of the first-order upwind method, while the other terms are all central difference scheme. Pressure is calculated based on the PIMPLE algorithm. The flow chart for the same is in Figure 2.1.

The approach approximates the Navier-Stokes equations to converge the solution using a predetermined amount of correction loops. This process continues until the maximum number of iterations or the given tolerance for the estimated parameter is reached. In order to achieve this, it first predicts the velocities, corrects the pressure and velocity, and then solves the turbulence model.The correction approach corrects the velocities by solving the incompressible Navier-Stokes equations and deriving a pressure transport equation based on the pressure Poisson equations. This approach is used to compute the pressures at the cell center and the velocity fluxes at the cell boundaries. The continuity equation and volume conservation are upheld when the flux in the first corrector iteration is derived from the preceding time step. The mathematical derivation of this method is described in more detail in Goeree et al.[5] and Issa, [6].

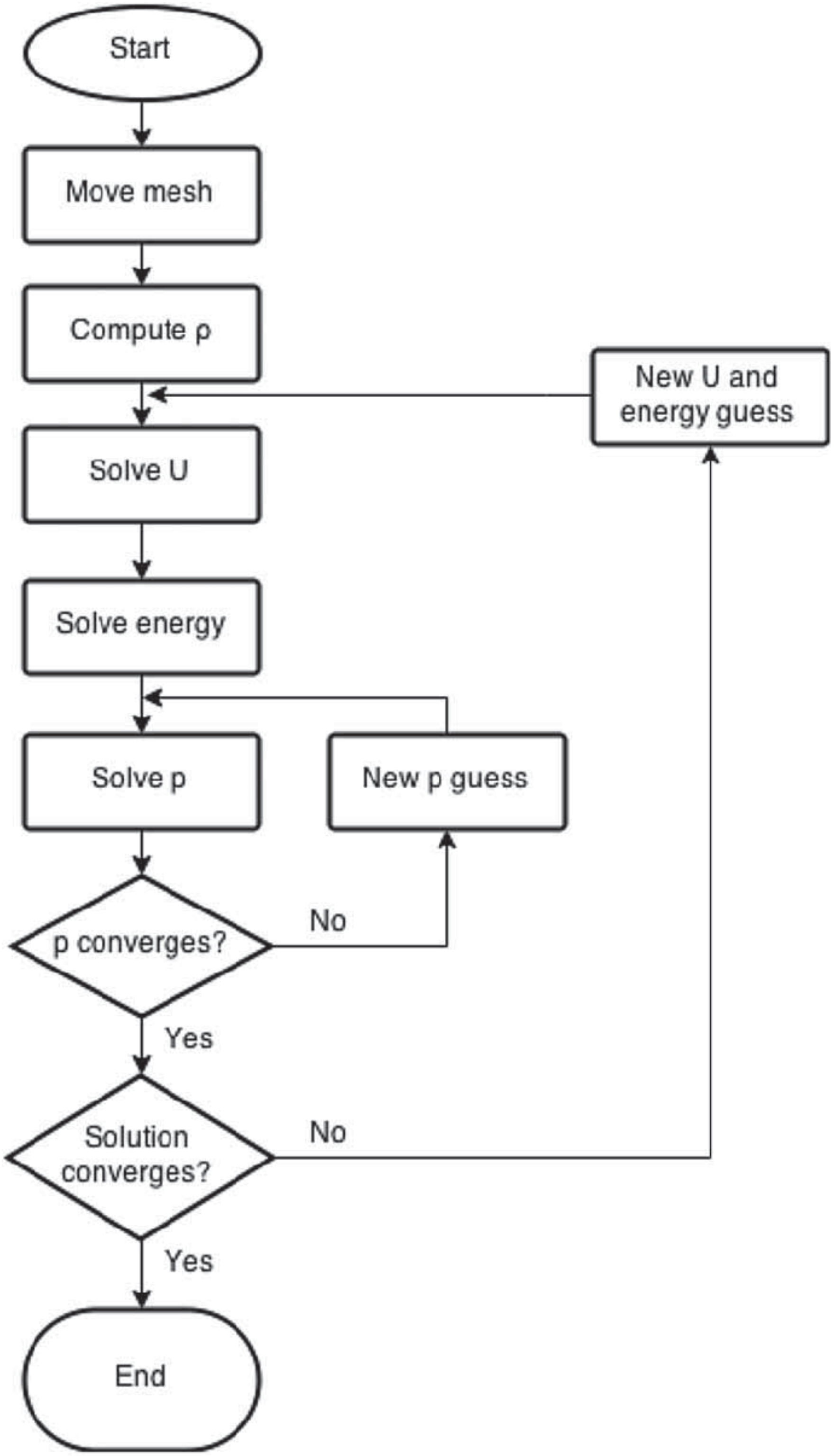

Figure 2.1: Flow chart of the PIMPLE algorithm [7]

2.4 Scope of this thesis

The study of bluff body flows will be this work's main emphasis, accompanied by synthetic turbulence techniques. In-depth numerical simulations will be used in this research to examine the intricate fluid dynamics surrounding bluff solids like spheres and cylinders. The main goals are to understand flow mechanics, define wake dynamics, and evaluate how well synthetic turbulence approaches capture turbulent phenomena. The research aims to shed light on the limitations and effectiveness of existing synthetic turbulence techniques inside the computational framework. This will enable a more thorough understanding of the techniques' applicability in real-world engineering simulations. This work will not engage in creating or exploring novel turbulence generation approaches.

Chapter 3

Flow over a cylinder

Vortex shedding has been studied through simulations for flow over a cylinder at a Reynolds number (Re) of 100. The numerical results obtained from these simulations have been validated against existing literature.

3.1 Simulation setup

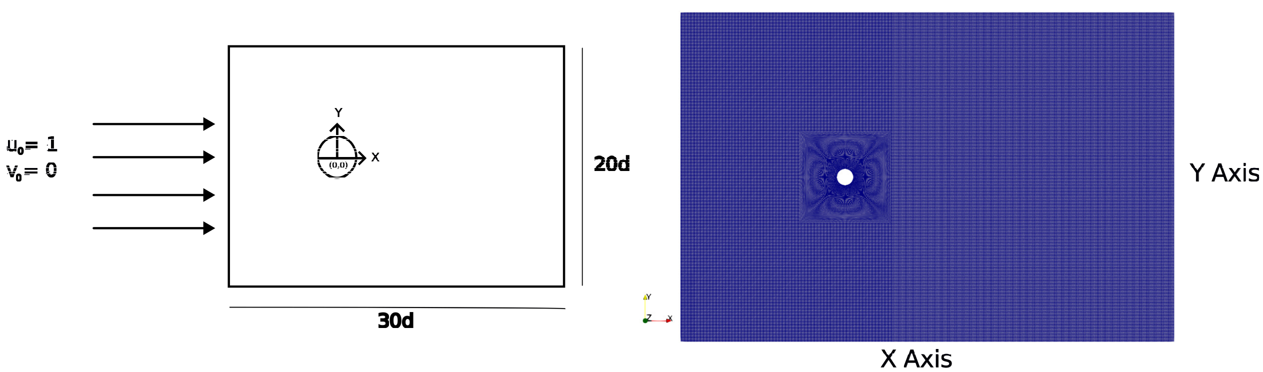

Figure 3.1: (left) Computational domain , (right) computational mesh

The two-dimensional computational domain is centered at the origin (0,0). The centre of this domain is where the cylinder of diameter $d = 1$ is placed. The computational domain's dimensions extend 30d and 20d, respectively, in the stream-wise and cross-stream directions. A structured grid with dimensions of 98×72 grid points is used to discretize the computing domain.

The inflow velocity applied is $(u_0, v_0) = (1, 0)$. Neumann boundary condition is enforced on the pressure field, ensuring a zero-gradient pressure condition along the inflow boundary. The outflow is described with advective condition for velocity, i.e. $\frac{Du}{Dt} = 0$, or $\frac{\partial u}{\partial t} + u_{\text{adv}} \cdot \frac{\partial u}{\partial x} = 0$, where

u_{adv} is the advective velocity which is set as $u_{\text{adv}} = 0.8 \cdot u_0$, and the pressure is Dirichlet condition with zero value. At the top and bottom, free slip condition is used. Finally, a no-slip condition is enforced on the bluff body boundary, where the fluid's velocity relative to the body's surface is zero.

Table 3.1: Boundary conditions implemented for the simulation

Face	**Boundary condition**
Inflow	$u_0 = 1; v_0 = w_0 = 0; \frac{\partial p}{\partial x} = 0$
Cylinder	$u = v = w = 0; \frac{\partial p}{\partial \eta} = 0$ (where η denotes normal to the cylinder surface)
Top and bottom walls	$v = 0, \frac{\partial u}{\partial y} = \frac{\partial w}{\partial y} = \frac{\partial p}{\partial y} = 0$
Outflow	$\frac{Du}{Dt} = 0, u_{\text{adv}} = 0.8 \cdot u_0,\ p = 0$

3.2 Results

The results found for the simulation of flow past a cylinder in two dimensions have been discussed.

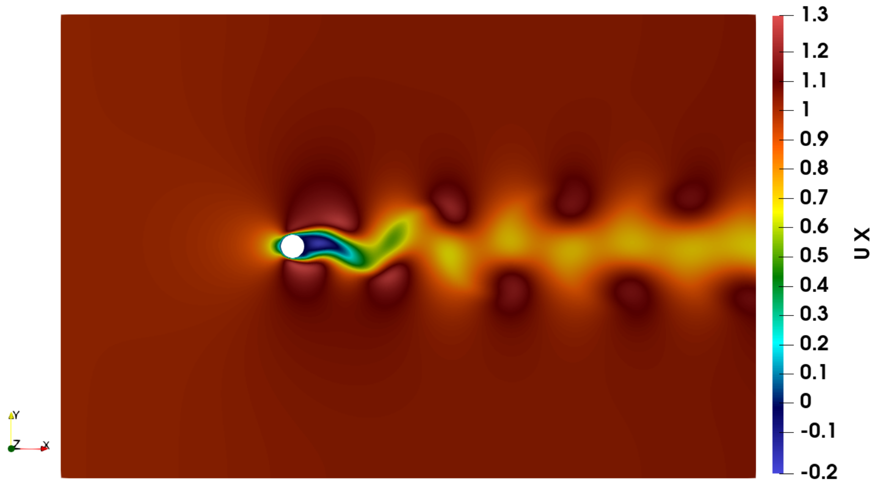

Figure 3.2: Instantaneous stream-wise velocity profile for $Re = 100$

Figures 3.2 and 3.3 show the instantaneous stream-wise velocity and span-wise vorticity components of the fully developed vortex shedding phenomenon at $Re = 100$, where the flow around the cylinder exhibits periodic shedding of vortices. This shedding is distinguished by a specific frequency linked with the shedding process, known as the shedding frequency. At Reynolds num-

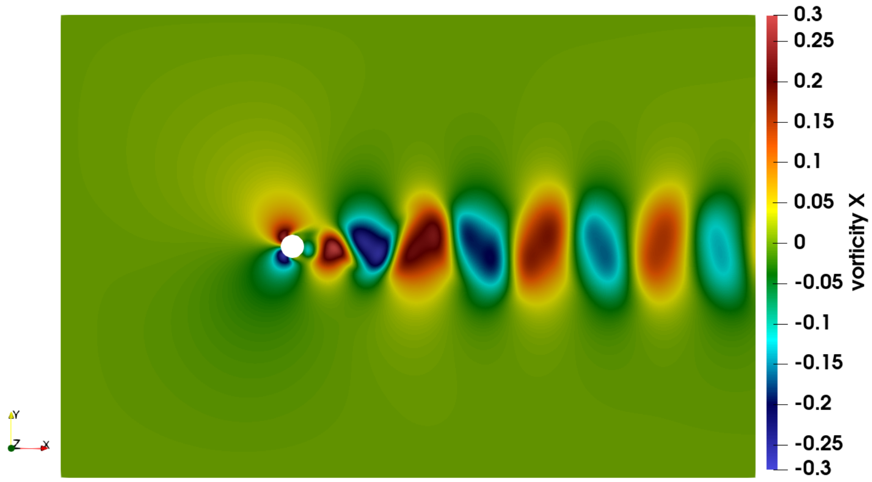

Figure 3.3: Instantaneous span-wise vorticity profile for $Re = 100$

ber $Re = 100$, the shedding frequency becomes steady, suggesting the formation of a periodic flow pattern around the cylinder.

3.2.1 Grid sensitivity study

A grid sensitivity study involves systematically varying the grid size while keeping other simulation parameters constant to evaluate its impact on the accuracy and convergence of numerical results. This helps determine the optimal grid size that provides accurate and converged results while minimizing computational cost and validating results against experimental or analytical data.

The grid sensitivity study was conducted by increasing the initial mesh size, referred to as Mesh 1, which had a total grid count of 98×72. This mesh was refined twice, doubling the number of grid points each time, resulting in Mesh 2 (196×144) and Mesh 3 (392×288). To verify and validate the results obtained from the refined meshes, surface pressure data was collected from the computational simulations and compared against experimental data. This comparison involved plotting the surface pressure distribution against the angular position around the cylinder for each refined mesh, alongside corresponding experimental measurements [8] (see Figure 3.4), where $C_p = \frac{p - p_ref}{\frac{1}{2}\rho U^2}$ is the pressure coefficient, and p_{ref} is the spatially averaged pressure from the inlet surface. The polar angle from the frontal stagnation point in the figure is denoted by θ.

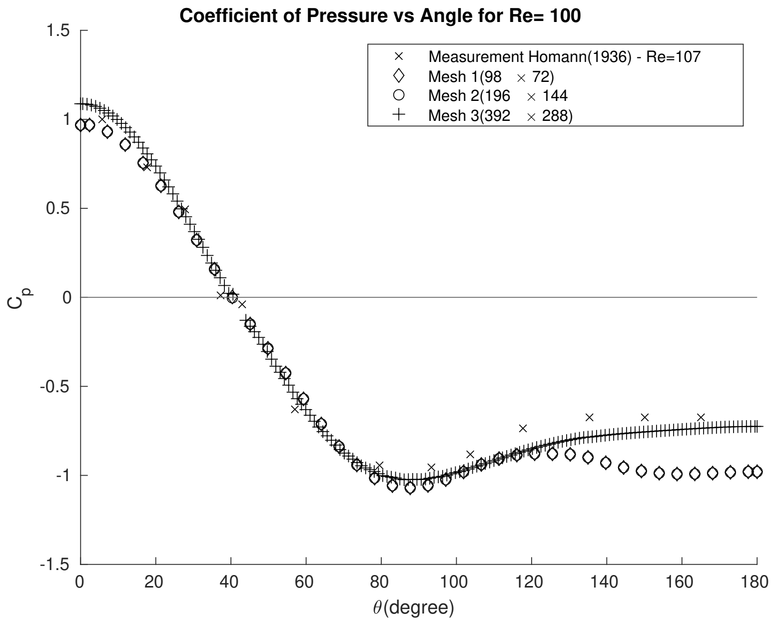

Figure 3.4: Surface pressure around the cylinder

3.2.2 Signal analysis

The cross-stream velocity data collected from the probe location present at (3,0,0) underwent analysis to determine the dominant frequency associated with the vortex-shedding phenomenon. This method divided the time-history data into smaller categories based on the number of observed shedding cycles. A shedding cycle is a characteristic oscillation pattern observed in the wake of a bluff body, such as a cylinder, in which vortices are repeatedly shed into the downstream flow. In this study, 15 shedding cycles were investigated. Fast Fourier Transform (FFT) analysis was carried out on each subset to determine the dominating frequency associated with vortex shedding.

The statistical stationarity process was employed to ascertain the dominant frequency accurately. This includes determining if the dominant frequency is consistent over different subsets of the sample or shedding cycles. When the dominant frequency stabilizes and no longer varies considerably in relation to the number of datasets or shedding cycles, it is considered the real dominant frequency linked with the vortex shedding phenomena. This means that the flow dynamics have stabilized, and the indicated dominant frequency appropriately characterizes the fundamental physics of vortex shedding.

The Strouhal number, which corresponds to the dominant shedding frequency, was found to be 0.1709 in this investigation. This value corresponds to the peak observed in Figure 3.5, representing the dominant shedding frequency. Table 3.1 compares the Strouhal numbers obtained in this study with those from various other studies on flow over a cylinder.

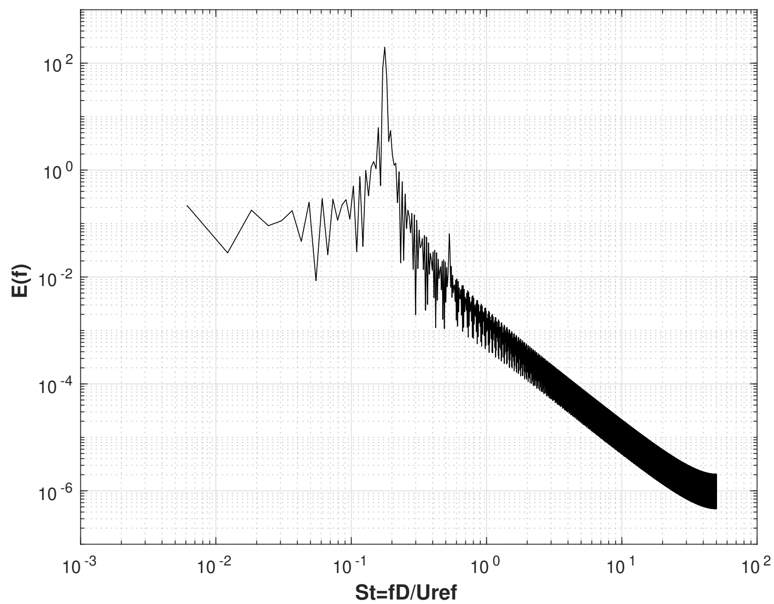

Figure 3.5: Fourier Spectrum at probe location = 3D, Strouhal number = 0.1709

Table 3.2: Strouhal Numbers comparison for $Re = 100$

Method/Study	**Strouhal Number**
Berger & Wille [9] (Expt.)	0.16–0.17
Roshko [10] (Expt.)	0.167
Williamson [11] (Expt.)	0.164
Braza et al. [12] (FVM)	0.16
Senocak & Shyy [13] (FVM)	0.164
Present Study (FVM)	0.1709

3.3 Summary

The result for the Strouhal number reasonably matches the literature. The wake at $Re = 100$ becomes unstable, oscillating with a specific frequency. From the grid sensitivity study, Mesh 3 matches the experimental measurement more. The validation and grid independence study has been conducted by plotting the pressure coefficients at different angles. The Strouhal number and pressure coefficients have been compared with the benchmark.

Chapter 4

Inflow perturbation techniques

4.1 Introduction

With the advancement of eddy-resolving simulation techniques like large-eddy simulation (LES), direct numerical simulation (DNS), and hybrid Reynolds-averaged Navier-Stokes (RANS)-LES, there has been a growing need for accurate inflow turbulence generating methods. These methods quantify the stochastic features of turbulent eddies of various sizes, as well as their statistical spatial and temporal coherence. The challenge of precisely prescribing turbulent eddies at the inlet boundary of spatially expanding turbulence simulations is crucial for obtaining unsteady computational solutions.

Precise input turbulence generation is essential for investigating transition and turbulence physics, simulating complex turbulent flows, and forecasting flow device performance in the fields of aerodynamics, atmospheric science, computational wind engineering, and computational aeroacoustics. For eddy-resolving simulation algorithms, this dual nature of concurrent randomness and coherence associated with turbulent eddying motion poses challenges, especially close to the intake border of spatially evolving turbulence simulations.

Generating inflow turbulence has several issues, including assuring precise prescription of turbulent eddies, maintaining spatial homogeneity, and matching grid resolution and Reynolds number across computational domains. Furthermore, spurious periodicity can emerge in strong recycling systems, producing unphysical, theoretically consistent, but physically nonsensical streamwise repeated patterns.

4.2 Methods of Inflow turbulence generation

The methods of generating inflow boundary conditions for LES and DNS are reviewed here, primarily with respect to their computational cost, the information needed for them to function, the turbulent flow field they produce, and their effect on the downstream flow.

4.2.1 Precursor simulation technique

An approach that establishes starting or boundary conditions for a primary simulation is known as precursor simulation. The precursor simulation is a separate simulation that is run so that dynamics or upstream flow conditions that affect the main simulation area can be recorded. The precursor simulation provides instantaneous velocity fluctuations in a plane at a fixed stream-wise point, which are then specified at the main simulation's inlet at each time step, as seen in Fig. 4.1.

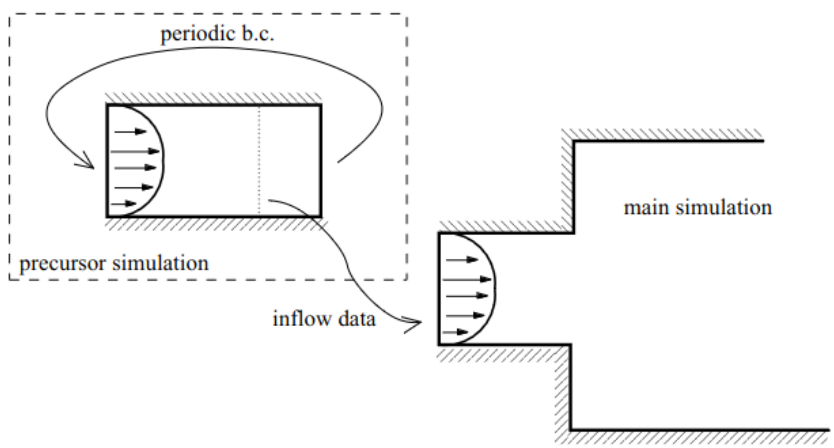

Figure 4.1: Sketch of a LES using a precursor simulation dedicated to the generation of the inflow data.

Implementation

The implementation of the precursor simulation technique typically involves the following steps:

1. Choose the area of interest for the primary simulation and determine the upstream flow to be recorded.

2. Assembling the upstream region of interest into a separate computational domain to run the precursor simulation.

3. Define appropriate boundary conditions for the precursor simulation domain based on the desired flow behaviour or boundary conditions.

4. Run the precursor simulation to collect flow data at the main simulation domain's boundary or inlet, such as pressure, velocity, and turbulence characteristics.

5. Apply the results of the precursor simulation as the main simulation's initial or boundary conditions.

Advantages

The precursor simulation technique has many advantages:

- It provides the main simulation's more accurate and realistic initial or boundary conditions.
- Also allows for better control over upstream flow conditions, which leads to improved simulation accuracy.
- And enables the simulation of transient or unsteady flow phenomena originating upstream of the main simulation domain.

This approach was adopted by Friedrich and Arnal [14] and Kaltenbach et al. [15] to generate inflow data for an LES of a plane diffuser and an LES of a backward-facing step, respectively, by extracting velocity planes from a preceding periodic channel flow. Breuer and Rodi [16] used a precursor simulation of a periodic square duct flow to generate inflow data for LES of a 180° curve. By simulating two periodic coaxial pipe flows, Akselvoll and Moin [17] generated inflow data for the intake section of the LES of a coaxial jet combustor.

4.2.2 Recyling method

In contrast to precursor simulation, the recycling approach recycles flow information from the exit or very near the end of the simulation domain back to the inlet, hence preserving a statistical steady state within the same simulation region. Lund et al. [18] introduced this technique, putting zero pressure gradient boundary layer for inlet situation.

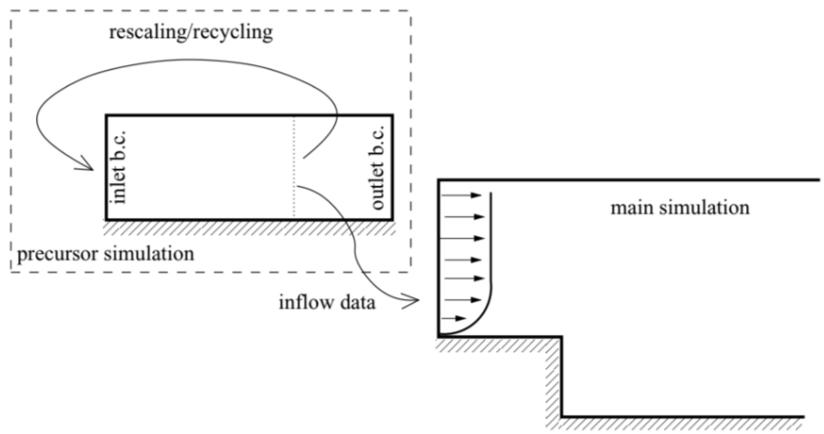

Figure 4.2: Schematic showing the Lund et al. [18] rescaling/recycling technique used to create the inlet conditions for a boundary layer with no pressure gradient.

Implementation

This method typically involves the following steps :

1. By employing the velocity in a plane (the rescaling station) located at multiple boundary-layer thicknesses downstream of the inlet, the method assesses the velocity signal at the inlet plane.

2. The mean and fluctuation components of the velocity field are separated at the rescaling station.

3. The mean and fluctuation components in the inner and outer layers are scaled separately to accommodate for the different similarity laws in these two places.

4. As a boundary condition at the entrance, the rescaled velocity is eventually reintroduced.

Advantages

- Reusing flow data saves much computing expense by removing the requirement to recalculate the whole flow field for every simulation.
- A smoother transition between time steps or iterations is one way that recycling flow data might stabilize the simulation.
- Maintaining uniform boundary conditions throughout successive simulations through the reuse of flow data increases the accuracy of the results.

The method was applied by Aider and Danet [19] to produce turbulent flow inlet conditions over a step that faces backward, and by Wang and Moin [20] to produce hydrofoil inlet conditions upstream of the trailing edge, in an area with a low-pressure gradient. Although the technique has only been used on equilibrium boundary layers thus far, Lund et al. [18] noted that by altering the rescaling process, it can be extended to non-equilibrium boundary layers that accelerate or decelerate boundary layers by simply changing the rescaling procedure. Though no results on the subject have been published, it is reported that simulations utilizing this modified version of the original approach appeared promising. Sagaut et al. [21] subsequently offered an extension of the original method of Lund et al. [18] to compressible turbulence. It takes advantage of pressure recycling and scaling.

Ferrante and Elghobashi [22] found that the flow field's initialization greatly affected the sensitivity of Lund's approach. The initialization procedure suggested by Lund et al. [18] (mean velocity profile superimposed with random uncorrelated fluctuations) did not allow them to produce fully developed turbulence. They proposed a more robust form of Lund's original method, which is covered in the following section, where the flow field is initiated by synthetic turbulence with a predefined energy spectrum and shear stress profile.

4.3 Synthetic turbulence

Inflow conditions are synthesized using a stochastic approach rather than a precursor simulation or the rescaling method. These stochastic procedures provide a random velocity signal that mimics turbulence using random number generators. These techniques are known as synthetic turbulence-generating techniques. They are predicated on the underlying premise that a series of low-order statistics can be repeated to mimic a turbulent flow.

These techniques can specify a variety of statistics, such as mean velocity, turbulent kinetic energy, Reynolds stresses, and correlations between two points and two times. However, the synthetic turbulence is simply a rough representation of the actual thing. Higher-order statistical terms, like the dissipation rate, turbulent transport, and pressure-strain term included in the budget of Reynolds stresses, are typically not reproducible from a statistical perspective.

A turbulent flow comprises several eddies of varying sizes, the shapes of which vary depending on the flow in question. It is predicted that the synthesized turbulence will go through a transition phase before redeveloping into a more physical form if the dynamics and structure of the turbulent eddies are not adequately replicated. Recently, there has been a proposal for a wide range of artificial turbulence production techniques. Some of the methods are discussed below :

Synthetic Random Fourier Method (SRFM)

This method utilizes Fourier space. It is a spectral technique that creates inflow turbulence by breaking down the signal into Fourier modes. It was initially created by Kraichnan [23]. An isotropic, three-dimensional, homogeneous synthetic velocity field was used to initialize the flow domain in order to study the diffusion of a passive scalar. Given that the signal is homogeneous in all three spatial directions, it can be decomposed in Fourier space,

$$u'(x) = \sum_k \hat{u}_k e^{-i\mathbf{k}\cdot\mathbf{x}} \tag{4.1}$$

where the wavenumber in three dimensions is k. A specified isotropic three-dimensional energy spectrum $E(|k|)$ determines the defined amplitude of each complex Fourier coefficient $\hat{u}_k$, with a random phase θ_k selected from a uniform distribution on the interval $[0,2\pi]$. The velocity field synthesized is as follows:

$$u'_(x) = \sum_k \sqrt{E(|k|)} e^{-i(k \cdot x + \theta_k)} \tag{4.2}$$

The resulting velocity field exhibits the statistical properties and stochastic nature of turbulence. The study of the temporal decay of homogeneous isotropic turbulence has made use of this technique to initialize velocity fields [24].

Synthetic Digital Filtering Method (SDFM)

This is a mixed method, involving both spectral method and an additional factor of filtering. With the use of digital filters and Fourier decomposition, Davidson [25] suggested a way to create inlet conditions for LES or DNS. Isotropic turbulent fluctuations, $\tilde{u}_i(x)^{(m)}$ are synthesized at each time step m independently of the previously created signals, following a method akin to Kraichnan's [23] original concept. An asymmetric time filter is used to filter the separate isotropic fluctuations generated at each time step m in time, resulting in correlations in time that are represented as,

$$u_i(x)^{(m)} = a\, u_i(x)^{(m-1)} + b\, \tilde{u}_i(x)^{(m)} \tag{4.3}$$

where a and b are filter coefficient. A target mean velocity profile is then overlaid with the generated fluctuations. Gaussian filter with random temporal sequence was convolved by B ´echara et al [26], to create temporal coherence. The method was subsequently expanded by Klein et al. [27] to include spatial coherence in initially random data points. To impose spatial correlation, they used comparable filtering techniques. They may produce synthetic turbulence with regulated spatial and temporal properties. This mixed method enables the creation of synthetic turbulence that demonstrates temporal and spatial coherence, enabling better realistic stochastics of turbulence.

Synthetic Volume Forcing Method (SVFM)

There have been ideas to accelerate the process of adaptation towards equilibrium turbulence because approximate inlet circumstances necessitate a transition region downstream of the intake to reach equilibrium.

The process of developing turbulence from either an upstream laminar velocity profile or a synthetically created pseudo-turbulent profile can be accelerated by incorporating well-designed synthetic body force terms into the Navier-Stokes equation system inside a control zone. Such body force terms should have just enough strength to induce a rapid transition while also being sufficiently mild to avoid leaving any discernible consequences in the turbulent zone downstream.

The fine-tuning of the body force terms is a crucial component of SVFM. However, they must not be too strong to leave observable traces in the downstream turbulent region nor too robust to cause a swift transition to turbulence. By maintaining the statistical qualities and coherent structures of the body forces while managing their intensity, SVFM enables the controlled generation of turbulent flows.

Random volume forcing in the wall-normal direction was utilized in DNS by Schlatter & Orlu [28] and Khujadze & Oberlack [29] to facilitate an upstream Blasius velocity profile and transition to a completely turbulent incompressible ZPGSFPBL.

4.3.1 Synthetic Eddy Method (SEM)

This is an algebraic method that uses physical space to create synthetic turbulence, as opposed to the other ways covered so far. This thesis is also based on one of the modifications to this method (divergence-free SEM).

Jarrin et al. [30] proposed this strategy. It consists of a series of steps that will be covered, as well as the mathematical underpinning behind it. The schematic of SEM is shown in figure 4.3.

- The integral length scale $(\sigma(x))$, mean velocity, and Reynolds stress which are the input parameter are evaluated using the information that is currently accessible, such as the RANS simulation or analytical calculations, on the set of points S .

- An eddy bounding box is defined given as,

$$B = \{(x_1, x_2, x_3) \in \mathbb{R}^3 : x_{i,\min} < x_i < x_{i,\max},\ i = 1,2,3\} \tag{4.4}$$

  where the synthetic velocity fluctuations are generated and $x_{i,\min} = \min_{x \in S}(x_i - \sigma(x))$ and $x_{i,\max} = \max_{x \in S}(x_i + \sigma(x))$.

- Random positions x^k and intensity α^k are assigned to each eddies.

- Calculation of velocity signal on the set of points of S, given by,

$$\mathbf{u} = \mathbf{U} + \frac{1}{\sqrt{N}} \sum_{k=1}^{N} c_k f_{\sigma(\mathbf{x})}(\mathbf{x} - \mathbf{x}_k) \tag{4.5}$$

where the c_k represents the eddies' respective amplitude and the x_k denotes the positions of the N eddies. The velocity distribution of the eddy at $\mathbf{x}_k$ is denoted by $f_{\sigma(\mathbf{x})}(\mathbf{x} - \mathbf{x}_k)$. Assuming that the length scale σ is the only factor influencing the differences in distributions across the eddies, f_σ defined as,

$$f_{\sigma(\mathbf{x})}(\mathbf{x} - \mathbf{x}_k) = \sqrt{\frac{V_B}{\sigma^3}} f\left(\frac{x - x_k}{\sigma}\right) f\left(\frac{y - y_k}{\sigma}\right) f\left(\frac{z - z_k}{\sigma}\right) \tag{4.4}$$

where the shape function f is present for all eddies and $[-\sigma, \sigma]$ is the compact support for f and has the normalization

$$\int_{\mathbb{R}} f^2(x)dx = 1$$

or only on its support

$$\int_{-\sigma}^{\sigma} f^2(x)dx = 1.$$

The amplitudes c_k are given by:

$$c_{ki} = a_{ij}\varepsilon_{kj}$$

where the Cholesky decomposition of the Reynolds stress tensor R_{ij} is represented by a_{ij} :

$$a_{ij} = \begin{pmatrix} \sqrt{R_{11}} & 0 & 0 \\ \frac{R_{21}}{a_{11}} & \sqrt{R_{22} - a_{21}^2} & 0 \\ \frac{R_{31}}{a_{11}} & \frac{R_{32} - a_{21}a_{31}}{a_{22}} & \sqrt{R_{33} - a_{31}^2 - a_{32}^2} \end{pmatrix} \tag{4.6}$$

and ε_{kj} are independent random variables drawn from any distribution with a zero mean and unit variance.

Jarrin et al. [30] suggested the function given as :

$$f(x) = \begin{cases} \sqrt{\frac{3}{2}}(1-|x|) & \text{if } |x| < 1 \\ 0 & \text{otherwise} \end{cases} \tag{4.7}$$

The intensities α_j are from a random number series with $\langle \alpha_j \rangle = 0$ and $\langle \alpha_j^2 \rangle = 1$. These conditions are taken into consideration from analysis of Reynolds stress field, which is generated by this method.

- Eddies get convected via the eddy box, by $\mathbf{x}_k = \mathbf{x}_k + \mathbf{U}_b \cdot \Delta t$,where $\mathbf{U_b} = \frac{\int_S u_{ds}}{\int_S ds}$ is the bulk velocity calculated from the average velocity given by the user.
- Eddies leaving bounding box gets regenerated at the opposite surface.
- **u** is calculated and superimposed onto **U** to generate the inlet condition.

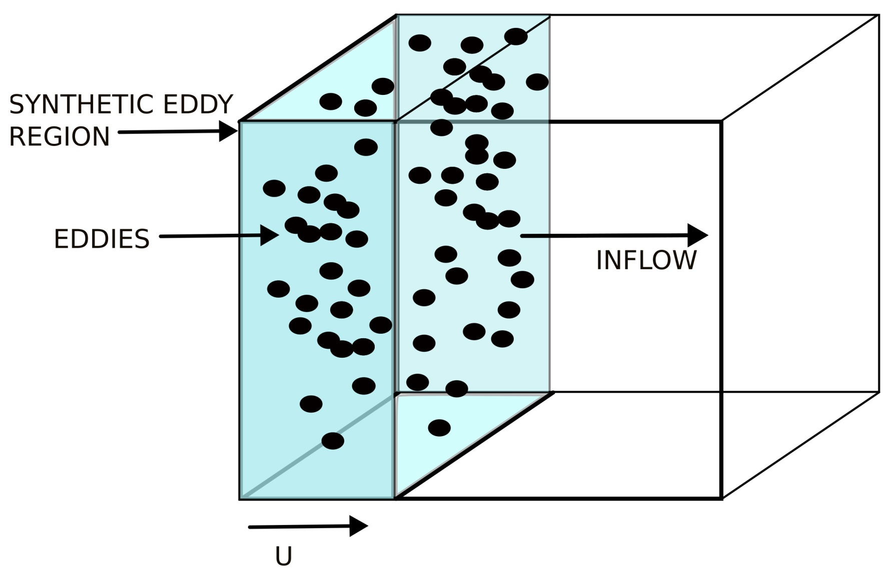

Figure 4.3: Schematic of SEM

Divergence Free Synthetic Eddy Method (DFSEM)

The SEM formulation allows for any chosen Reynolds stress field to be imposed (via the a_{ij} coefficients in equation 4.6), however the velocity field is not generally divergence-free.

Poletto et al. [31] proposed a methodology that involves applying the original SEM methodology to the vorticity field, which is then translated back to the velocity field by taking the curl of it.

$$\nabla \times \omega' = \nabla(\nabla \cdot \mathbf{u}') - \nabla^2 \mathbf{u}' \tag{4.8}$$

Since the flow considered is incompressible, first term could be removed, which results in Poisson equation for velocity field, which can be solved and gives the expression for velocity field fluctuation as:

$$\mathbf{u}'(\mathbf{x}) = \sqrt{\frac{1}{N}} \sum_{k=1}^{N} \frac{q_\sigma(|\mathbf{r}^k|)}{|\mathbf{r}^k|^3} (\mathbf{r}^k \times \alpha^k) \tag{4.9}$$

where $\mathbf{r}_k = \frac{\mathbf{x}-\mathbf{x}_k}{\sigma_k}$, $q_\sigma(|\mathbf{r}|_k)$ is an appropriate shape function, and α_k are random numbers with zero average which represents the eddy intensities.

A suitable shape function proposed by Poletto et al. is

$$q_i = \begin{cases} \sigma_i[1-(d_k)^2], & \text{if } d_k < 1 \\ 0, & \text{elsewhere} \end{cases} \tag{4.10}$$

Everywhere, the function q_i is continuous. For $d_k = 1$, on the other hand, its derivative is not exactly defined, and only a right- or left-sided derivative is defined. All places other than the eddy surface $d_k = 1$ are defined by the preceding formulation as having a divergence-free velocity field; however, significant issues are unlikely to result from this formal omission. This method has been incorporated into the solver as part of the mathematical foundation for solution.

Simulations are performed for the cylinder example, which was described in Chapter 3, as well as the sphere case, which will be discussed in the following chapter.

This chapter has outlined a wide range of techniques for producing input turbulence. The choice of one of these strategies for the current simulations is primarily based on how well it integrates with the solver architecture. Notably, in the context of OpenFOAM simulations, the divergence-free synthetic eddy method (DFSEM) is the most suitable option. This inclination stems from DFSEM's ability to provide strong adaptation within the solver framework, making it a well-known and preferred method for creating inflow turbulence in computational fluid dynamics research.

Chapter 5

Flow over a cylinder and sphere with DFSEM

5.1 Introduction

In this chapter, simulations of flow over a cylinder and a sphere will be discussed using the divergence-free synthetic eddy method (DFSEM), as discussed in Chapter 4.

5.2 Implementation of DFSEM

Turbulent intensity is given as,

$$I = \frac{\sqrt{\overline{u'u'}}}{U_\infty} \tag{5.1}$$

where $\overline{u'u'}$ represents the Reynolds-averaged velocity fluctuations in a turbulent flow, which denotes the fluctuating component of velocity in a particular direction, and the overbar represents a Reynolds averaging operation, and U_∞ is the flow velocity.

For the current two simulations, the turbulent intensity is set at $I = 0.1$ or 10%. Equation 5.2 represents the Reynolds stress with only the diagonal terms or the normal components present and are set to be equal while keeping the off-diagonal or shear terms at zero, treating the flow as homogeneous isotropic turbulence (HIT).

$$R = \begin{pmatrix} \overline{u'u'} & 0 & 0 \\ 0 & \overline{u'u'} & 0 \\ 0 & 0 & \overline{u'u'} \end{pmatrix} \tag{5.2}$$

Previous investigations have used this methodological framework to generate free-stream turbulence (FST). The synthetic digital filtering method (SDFM) [32] was employed to generate synthetic turbulence, briefly discussed in the previous chapter. It is crucial to note that while the approach for calculating Reynolds stress values is identical, there are distinct nuances and variances in the implementation and computing strategies used in various research.

5.3 Cylinder case

Simulations have been conducted to investigate the vortex shedding phenomenon for flow over a cylinder at a Reynolds number (Re) of 100 with inflow as turbulent using synthetic turbulence techniques. The numerical results obtained from these simulations have been validated against the simulation without inflow turbulence.

5.3.1 Simulation setup

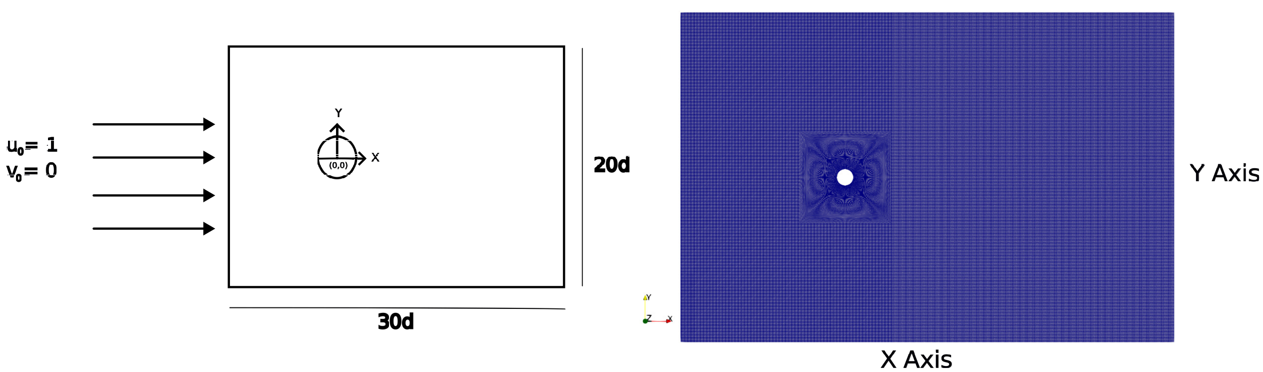

Figure 5.1: (left) Computational domain , (right) computational mesh

The computational domain remains consistent with the configuration utilized in Chapter 3, established in two dimensions and centred at the origin (0,0,0). The cylinder, characterized by a diameter $d = 1$, is positioned at the centre of this domain. The dimensions of the computational domain extend to 30d and 20d along the stream-wise and cross-stream directions, respectively. Following the outcomes of the grid sensitivity study performed in Chapter 3, the utilization of Mesh

3, which has a total grid count of 392×288, is favoured due to its alignment with experimental results.

Building upon the groundwork laid in Chapter 2, the simulation adopts the large eddy simulation (LES) framework, a methodology briefly introduced earlier. The LES model of choice for this simulation remains the Smagorinsky model, renowned for its efficacy in capturing turbulent flow phenomena. Notably, this model employs a constant eddy viscosity coefficient, which scales proportionally with the grid size. This inherent characteristic renders it computationally efficient, particularly for simulations conducted on large spatial scales.

Mathematically, the Smagorinsky model [33] expresses the residual stress tensor τ_{ij} as:

$$\tau_{ij} = -2\nu_t S_{ij} \tag{5.3}$$

where ν_t is the eddy viscosity, and S_{ij} represents the resolved strain rate tensor defined as:

$$S_{ij} = \frac{1}{2}\left(\frac{\partial u_i}{\partial x_j} + \frac{\partial u_j}{\partial x_i}\right) \tag{5.4}$$

The eddy viscosity ν_t is modeled as a product of a velocity scale and a length scale l_{LES} proportional to the filter size Δ through the Smagorinsky constant C_s given as: $l_{LES} = C_s\Delta$, and the eddy viscosity becomes:

$$\nu_t = (l_{LES})^2|\mathbf{S}| \tag{5.5}$$

$$\nu_t = (C_s\Delta)^2|\mathbf{S}| \tag{5.6}$$

Also, since the value of $\nu_t > 0$, it implies that the modelled turbulence remains positive throughout. The Smagorinsky model does not allow any backscatter from modelled to resolved regime.

To implement DFSEM, additional input parameters are given which are Reynolds stress, mean velocity and integral length scale, as discussed in chapter 3. For the current simulation the Reynolds stress value as calculated by keeping the turbulent intensity (I) of 0.1, is $\overline{u'u'} = 0.003334$, as shown in equation 5.3,

$$R = \begin{pmatrix} 0.003334 & 0 & 0 \\ 0 & 0.003334 & 0 \\ 0 & 0 & 0.003334 \end{pmatrix} \tag{5.7}$$

The eddy bounding box as discussed earlier in chapter 3, which corresponds to a set of points are also given. In total, 13 points with synthetic fluctuations are assigned. The points are from the inlet surface, with keeping the x co-ordinate same (i.e. $x = -10$), but varying the y co-ordinate as: $-10, -9, -8, -6, -4, -2, 0, 2, 4, 6, 8, 9, 10$ or the line equation $x = -10$ as shown in figure 5.2 which basically implies that the eddies are put along the white line.

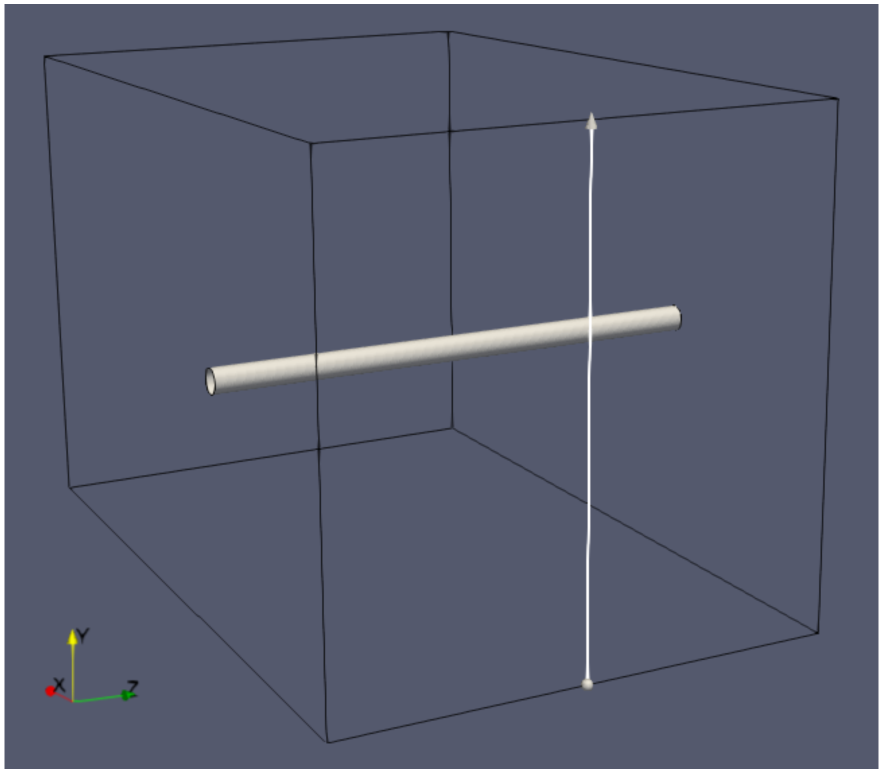

Figure 5.2: Eddies applied along the line in the inlet surface

The mean velocity applied is $(U,V) = (1,0)$, and the integral length scale is the cylinder diameter $d = 1$. The characteristic length scale is set to 1, and the ratio of the sum of eddy volumes to eddy box volume, also known as eddy density (fill fraction), is set to 1, with the number of eddies per cell set to 3.

The inflow velocity applied is $(u_0, v_0) = (1,0)$. Neumann boundary condition is enforced on the pressure field, ensuring a zero-gradient pressure condition along the inflow boundary. The outflow is described with advective condition for velocity, where u_{adv} is the advective velocity which is set as $u_{\text{adv}} = 0.8 \cdot u_0$, and the pressure is Dirichlet condition with zero value. At the top and bottom, free slip condition is used. Finally, a no-slip condition is enforced on the bluff body boundary, where the fluid's velocity relative to the body's surface is zero.

Table 5.1: Boundary conditions implemented for the simulation

Face	Boundary condition
Inflow	$u_0 = 1; v_0 = w_0 = 0; \frac{\partial p}{\partial x} = 0$ (DFSEM applied to inflow)
Cylinder	$u = v = w = 0; \frac{\partial p}{\partial \eta} = 0$ (where η denotes normal to the cylinder surface)
Top and bottom walls	$v = 0, \frac{\partial u}{\partial y} = \frac{\partial w}{\partial y} = \frac{\partial P}{\partial y} = 0$
Outflow	$\frac{Du}{Dt} = 0, u_{\text{adv}} = 0.8 \cdot U_0,\ p = 0$

5.3.2 Results

The results found for the simulation of flow past a cylinder in two dimensions with turbulent inflow has been discussed.

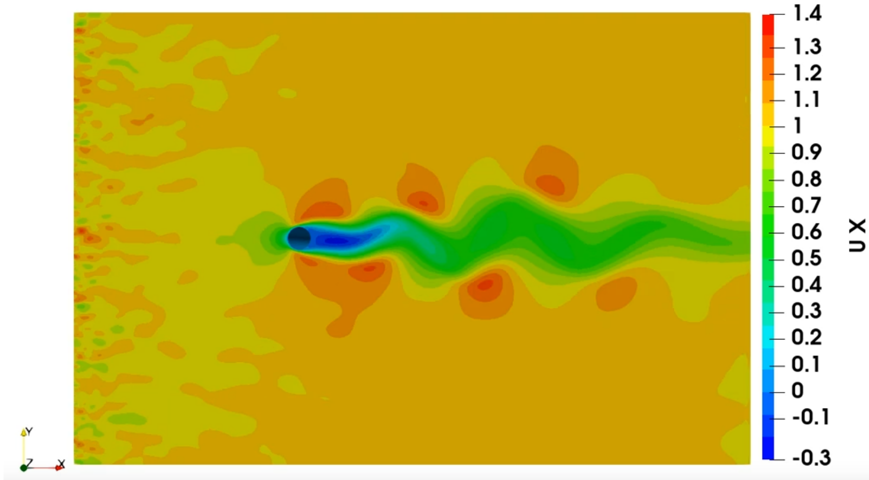

Figure 5.3: Instantaneous stream-wise velocity profile for $Re = 100$ with inflow perturbations

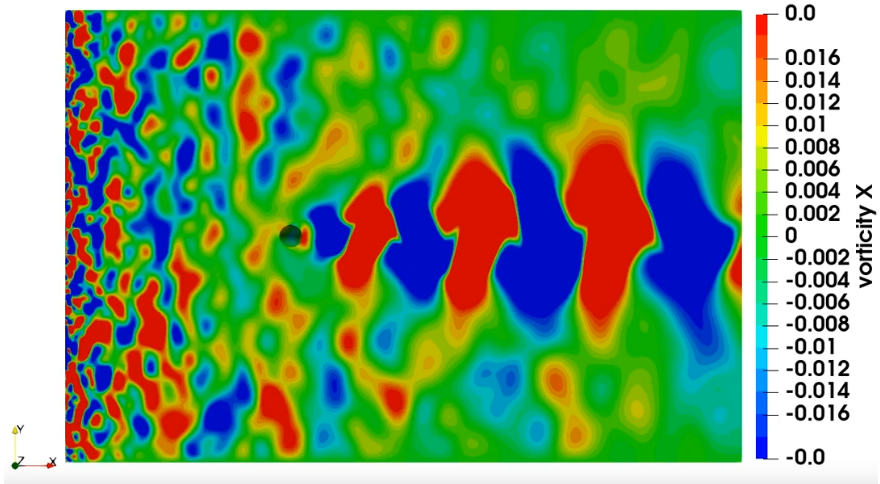

Figure 5.4: Instantaneous span-wise vorticity profile for $Re = 100$ with inflow perturbations

The wake instability behind the cylinder and the fully developed vortex shedding phenomenon at $Re = 100$ are shown visually in Figures 5.2 and 5.3, which are the instantaneous stream-wise velocity and stream-wise vorticity components, respectively. Although laminar flow is often observed at this Reynolds number, the method used in these simulations to create synthetic turbulence causes fluctuations in the inflow. Despite the nominal Reynolds number, the flow field is dynamic, as evidenced by the observed instability in the wake zone, partly caused by this turbulent inflow condition. In addition, as was discussed in Chapter 2, the shedding has a frequency attached to it.

Comparison with laminar flow

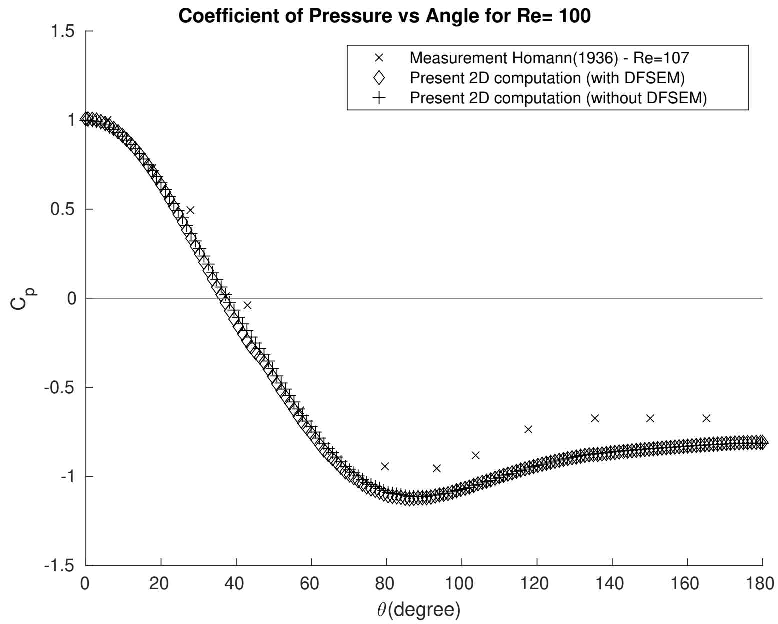

Figure 5.5: Surface pressure comparison with and without DFSEM

Plotting C_p vs θ to examine the profile with and without inflow perturbations is presented in Figure 5.4. As can be shown, the cylinder's surface pressure has not been significantly impacted by the input disturbances. For $Re = 100$, the two plots seem to be overlapping, along with the experimental measurement [8].

Signal analysis

For signal analysis, the same methodology as previously demonstrated in Chapter 3 was employed. The cross-stream velocity component has been collected at probe location $(3,0,0)$. In this study, 20 shedding cycles were selected to partition the time-series data into smaller subsets, and the Strouhal number computed was found to be 0.1717. Table 5.2 compares the value of the Strouhal number for the cylinder case, with DFSEM present and without it.

Table 5.2: Comparison of Strouhal Numbers for Cylinder Case

Simulation Condition	**Strouhal Number**
Without DFSEM	0.1709
With DFSEM	0.1717

Figure 5.6(left) depicts the time-series data for the cross-stream velocity, plotted against non-dimensional time. The graph clearly illustrates the periodic nature of the fluctuation signal, indicating that the vortex-shedding phenomenon is indeed periodic. This periodicity is a characteristic flow feature around bluff bodies, where vortices are shed periodically into the downstream flow, leading to oscillations in the velocity field.

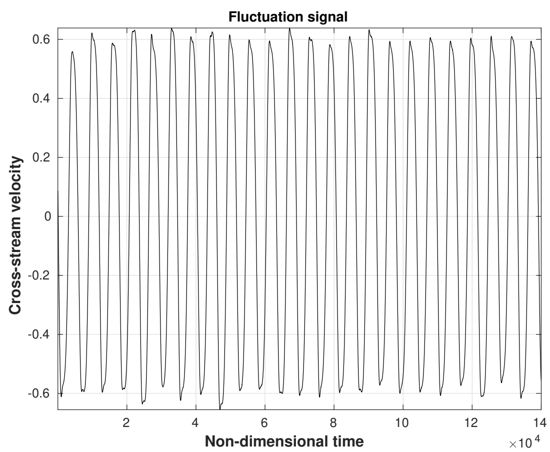

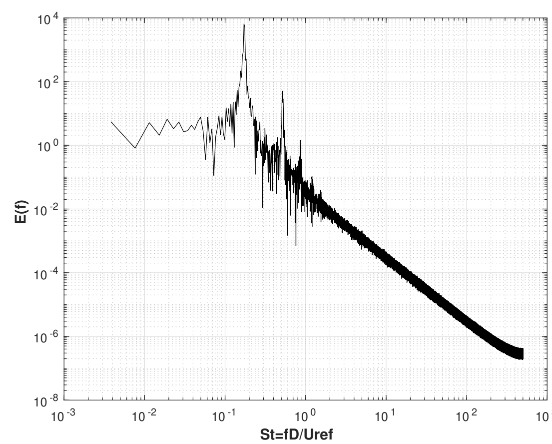

Figure 5.6: (left) time-history of cross-stream velocity , (right) Fourier Spectrum at probe location = 3D

Figure 5.7 shows how the energy value and the Strouhal number correspond to each other. The plot clearly shows a definite peak at a Strouhal number of 0.17, the typical frequency of the flow phenomenon considered in this simulation.

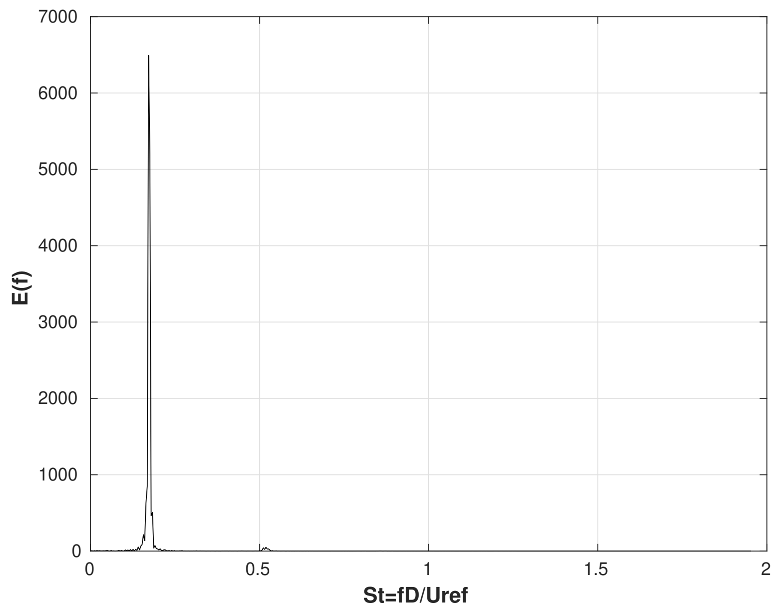

Figure 5.7: FFT of cross-stream velocity

5.3.3 Summary

The wake shows instability and oscillations with a specific frequency at a Reynolds number of 100. Despite applying DFSEM, the Strouhal number value for this simulation did not significantly alter.

5.4 Sphere case

Simulations are performed for flow over a sphere at $Re = 100000$ with inflow turbulence using DFSEM.

5.4.1 Simulation setup

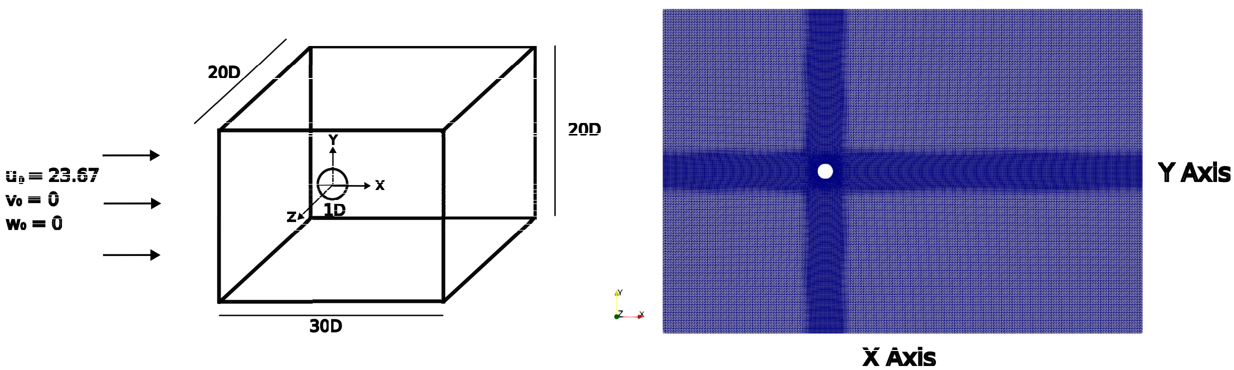

Figure 5.8: (left) computational domain , (right) Computational mesh

The computational domain is in three-dimension and is centered at the origin $(0,0,0)$. The sphere is positioned at the centre of the domain, with a diameter of $d = 0.062594$; the diameter taken into consideration is the diameter of a tennis ball (as seen in figure 5.8(left). The dimension of the computational domain extends to 30d in stream-wise direction, 20d in cross-stream direction and 20d in span-wise direction. The total grid count is $220 \times 160 \times 160$.

Table 5.3: Boundary conditions for sphere case

Face	**Boundary condition**
Inflow	$u_0 = 23.67; v_0 = w_0 = 0; \frac{\partial p}{\partial x} = 0$ (DFSEM applied to inflow)
Sphere	$u = v = w = 0; \frac{\partial p}{\partial \eta} = 0$ (where η denotes normal to the sphere surface)
Top and bottom walls	$w = 0, \frac{\partial u}{\partial z} = \frac{\partial w}{\partial z} = \frac{\partial p}{\partial z} = 0$
Front and back walls	$v = 0, \frac{\partial u}{\partial y} = \frac{\partial w}{\partial y} = \frac{\partial p}{\partial y} = 0$
Outflow	$\frac{Du}{Dt} = 0, u_{\text{adv}} = 0.8 \cdot u_0,\ p = 0$

The simulation is conducted within the LES framework, wherein the subgrid-scale (SGS) model is employed as a one-equation model present in the solver. (more details on the model are available in here. [34])

DFSEM is implemented with the same treatment as done in the previous section. The Reynolds stress value as calculated by keeping the turbulent intensity (I) of 0.1, is $\overline{u'u'} = 1.86756301$, as shown in equation 5.8,

$$R = \begin{pmatrix} 1.86756301 & 0 & 0 \\ 0 & 1.86756301 & 0 \\ 0 & 0 & 1.86756301 \end{pmatrix} \tag{5.8}$$

The eddy bounding box employed has been given 13 points to which synthetic fluctuations are assigned, for which the location of the points on the inlet surface, with the x-coordinate kept constant at $x = -0.661017$, while the y-coordinate varies according to the following values: -0.6, -0.5, -0.4, -0.3, -0.2, -0.1, 0, 0.1, 0.2, 0.3, 0.4, 0.5, 0.6. This arrangement corresponds to the line equation $x = -0.661017$.

The mean velocity applied is $(U,V,W) = (23.67,0,0)$, and the integral length scale is the sphere's diameter, $d = 0.62594$. The characteristic length scale is set to 1, the eddy density is set to 1, and the number of eddies per cell is 3.

The inflow velocity applied is $(u_0, v_0, w_0) = (23.67,0,0)$. Neumann boundary condition is enforced on the pressure field, ensuring a zero-gradient pressure condition along the inflow boundary. The outflow is described with the advective condition for velocity, and the pressure is a Dirichlet condition with zero value. At the top and bottom, free slip condition is used. Also, for the front and back, free slip condition is employed. Finally, a no-slip condition is enforced on the bluff body boundary, where the fluid's velocity relative to the body's surface is zero.

5.5 Results

The results obtained for the simulation of flow past a sphere in three-dimensional domain with turbulent inflow has been discussed.

The effect of synthetic turbulence implemented at the inlet can be understood by examining Figures 5.9 and 5.10, illustrating the instantaneous profiles of stream-wise velocity and stream-wise vorticity across the domain. These visual representations provide insight into how the applied turbulence influences the flow characteristics within the computational domain.

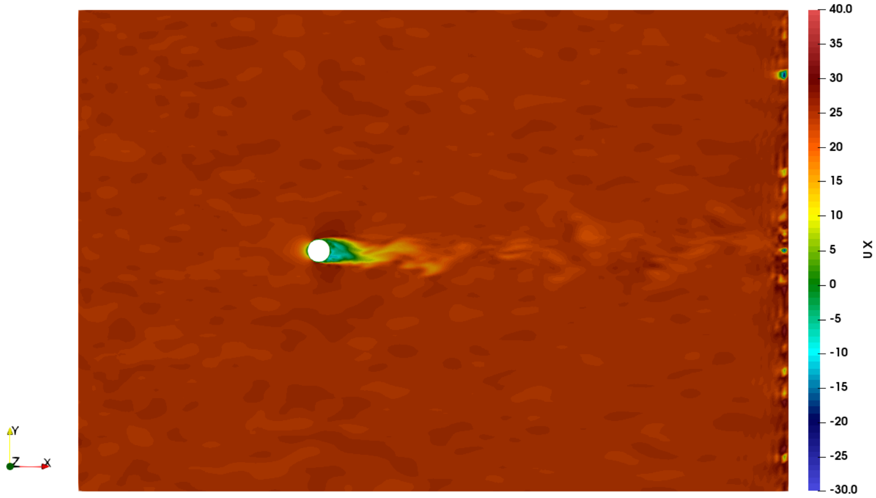

Figure 5.9: Instantaneous stream-wise velocity profile with inflow perturbations

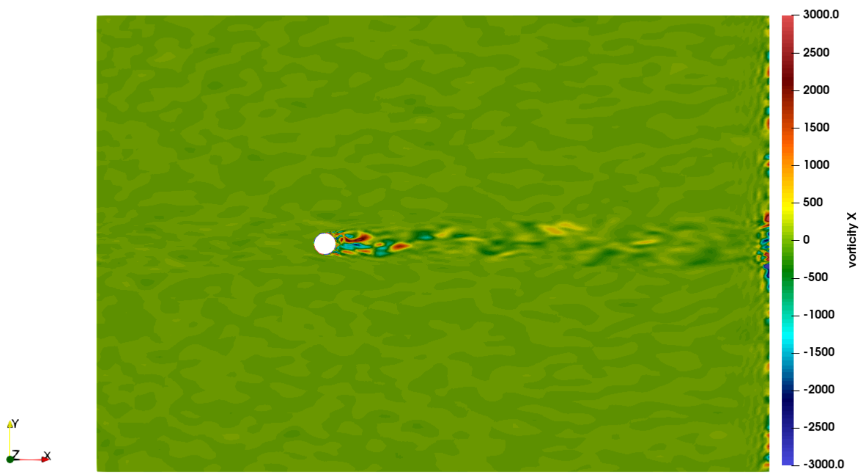

Figure 5.10: Instantaneous stream-wise vorticity profile with inflow perturbations

Figure 5.11 depicts an elaborate 3D turbulent vortical structure, with colour representing stream-wise vorticity. Notably, this depiction shows a helical structure in the wake trailing behind the sphere. This helical pattern symbolizes the complicated interaction of vortices and flow dynamics in the wake zone.

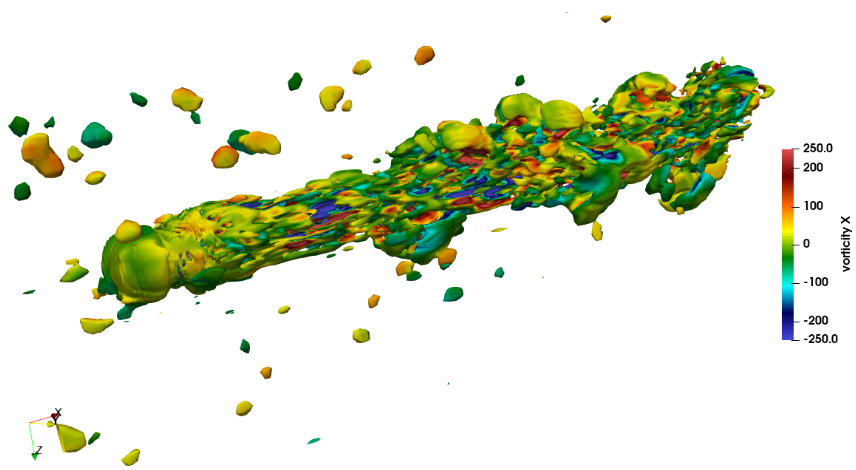

Figure 5.11: Iso-surface coloured by stream-wise vorticity

5.5.1 Validation with literature

Figure 5.12 shows the plot of the pressure coefficient averaged in time along the sphere. The plot also includes experimental data as references from Achenbach [35] and Constantinescu et al. [36].

Force coefficients

Figure 5.13 depicts the change of drag coefficient and lift coefficient over time; the mean drag coefficient is 0.4274, and the mean lift coefficient is 0.0129. The experimental values vary from 0.45 – 0.52 [35].

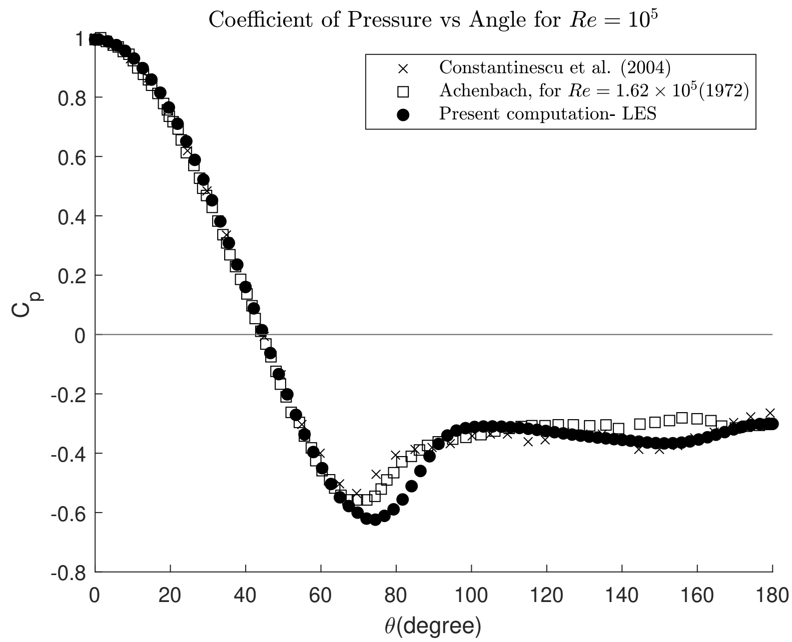

Figure 5.12: Surface pressure for sphere at $Re = 10^5$

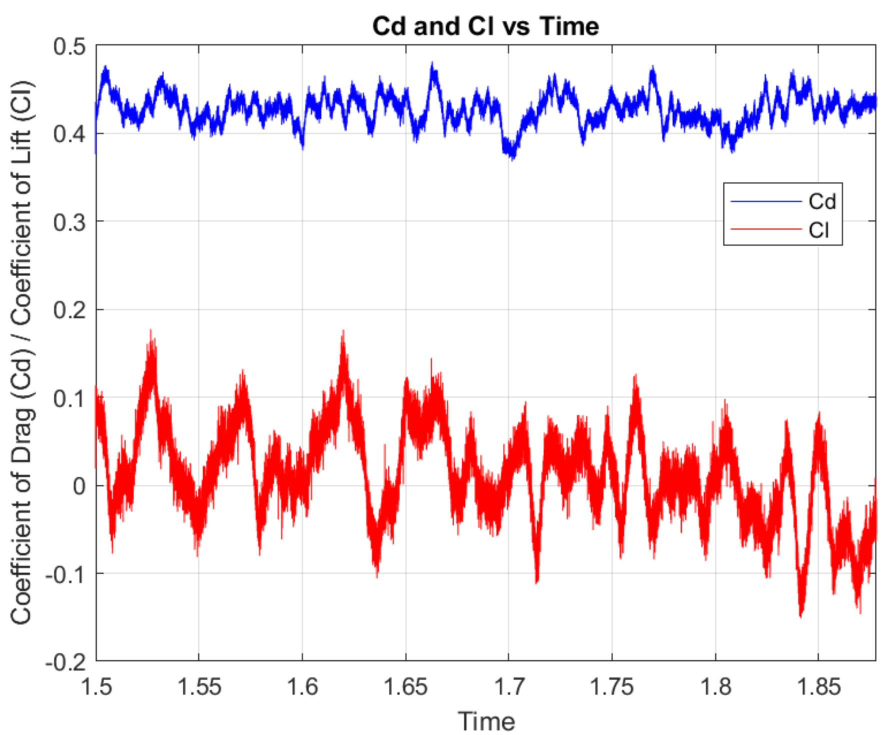

Figure 5.13: Force coefficient C_d and C_l

5.5.2 Signal analysis

For signal analysis, at probe location $(1.8, 0, 0)$, which corresponds to $3d$, the cross-stream velocity component has been collected. In this study, 20 shedding cycles were selected to partition the time-series data into smaller subsets,and the Strouhal number computed was found to be 0.1928 (see figure 5.14). Also, Strouhal number comparison at high Reynolds number is shown in table 5.4.

Table 5.4: Strouhal Numbers comparison for high Reynolds number $(> 10^4)$

Method/Study	**Strouhal Number**
Constantinescu et al. (RANS, DES) [36]	0.195
Muto et al. (LES) [37]	0.18
Achenbach (Experimental) [38]	0.189
Present Study (LES)	0.1928

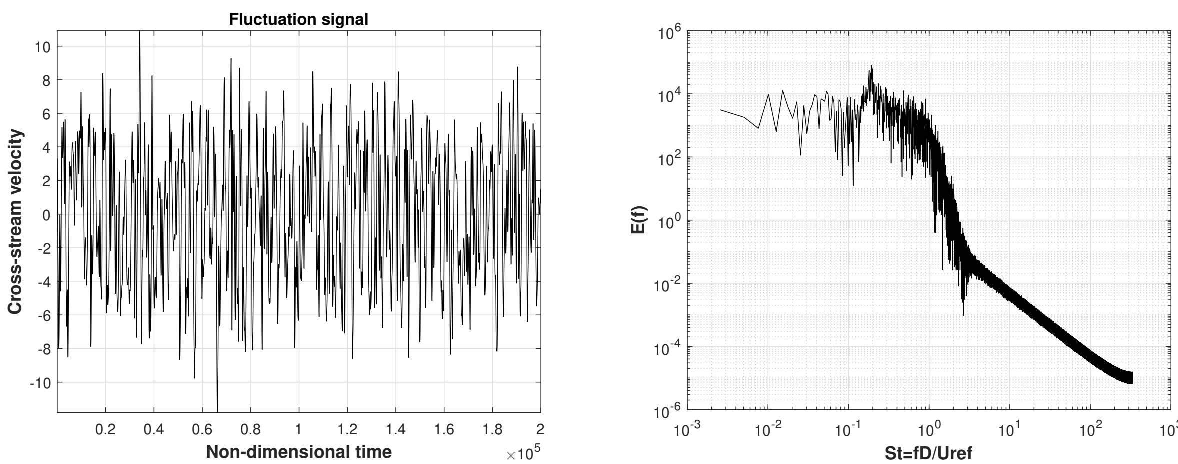

Figure 5.14: (left) time-history of cross-stream velocity , (right) Fourier Spectrum at probe location = 3d

Figure 5.15 shows how the energy value and the Strouhal number correspond to each other. The plot clearly shows a definite peak at a Strouhal number of 0.19.

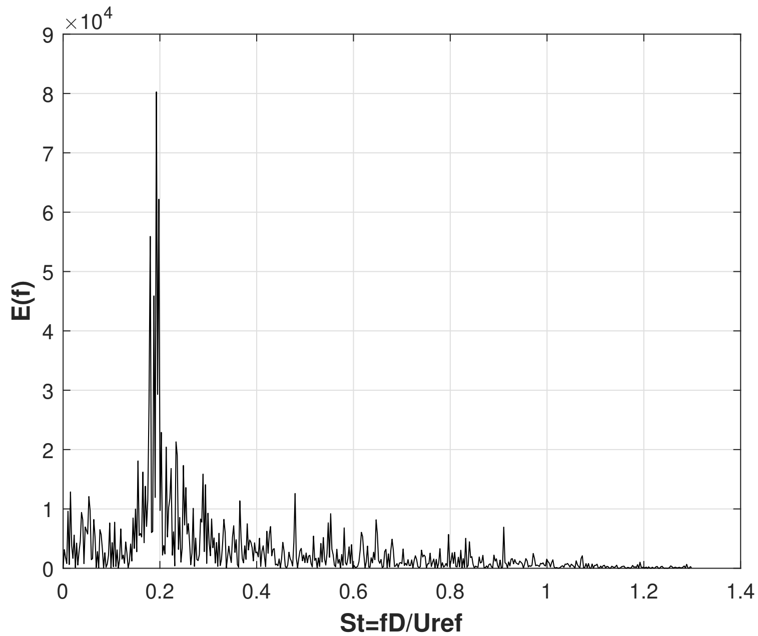

Figure 5.15: FFT of cross-stream velocity

5.5.3 Summary

The study of flow past a sphere, notably using DFSEM, has provided new insights into the underlying fluid phenomena. Notably, the wake trailing the sphere has a characteristic helical pattern attributed to the flow-sphere interaction.

It is worth noting that, despite using DFSEM, the resulting Strouhal number is 0.1928, comparable to the smooth case with no inflow disturbances. This parity emphasizes the delicate balance between natural flow properties and the influence of synthetic turbulence, implying that some flow features resist perturbations caused by DFSEM.

Furthermore, a thorough comparison of key aerodynamic parameters, such as the pressure, drag, and lift coefficients, was made with available literature. This rigorous study validates the numerical simulations and provides valuable insights into the computational model's accuracy and fidelity in capturing complex flow phenomena.

Chapter 6

Conclusion

This thesis used detailed simulations to explore the flow properties of a cylinder and a sphere. The primary goal was to analyze the effect of the divergence-free synthetic eddy method (DFSEM) on flow behaviour, particularly in scenarios with varying Reynolds numbers.

Simulations for the cylinder case were done at $Re = 100$. Both examples, with and without DFSEM, were investigated better to understand the effect of synthetic turbulence on flow dynamics. Turbulence intensity was set to 10% to provide uniformity between simulations using DFSEM.

Only DFSEM simulations were run in the sphere example, and these were done at a much higher $Re = 100,000$. This scenario aimed to investigate the suitability and efficacy of DFSEM in representing turbulent behaviour at high Reynolds numbers.

The results of the simulations showed that, in contrast to situations without DFSEM, the use of DFSEM did not significantly alter mean flow behaviour. In both cases, the mean flow properties were essentially the same, even with the addition of synthetic turbulence and changes in its severity.

The absence of significant variations implies that DFSEM, although a viable technique for producing artificial turbulence, might have little impact on mean flow behaviour in the circumstances investigated in this work. More research might be necessary to properly evaluate DFSEM's effectiveness in improving flow simulations, possibly using a more comprehensive range of Reynolds numbers or different turbulence production techniques.

Overall, this study's findings expand our knowledge of turbulent flow phenomena and the function of artificial turbulence techniques in computational fluid dynamics simulations. These results set the foundation for further studies on improving our understanding of complex fluid flow processes and turbulence modelling methods.

Chapter 7

Future Work

While this thesis has provided useful insights into the behaviour of turbulent flows over cylindrical and spherical geometries, there are various options for future research that can be pursued to build on the existing discoveries and answer outstanding issues. Here are some potential directions for further work:

1. **Impact of DFSEM at Higher Reynolds Numbers:** Investigate the effect of DFSEM on flow behaviour at higher Reynolds numbers. Conduct simulations over a broader range of Reynolds numbers to see if DFSEM has more pronounced effects in different flow regimes.

2. **Effect of Turbulence Intensity Variation:** In DFSEM, systematically alter the turbulence intensity parameter to assess its impact on flow characteristics. Determine how variations in turbulence intensity affect flow stability, vortex shedding, and other essential flow characteristics. Given that the thesis only considered the turbulent intensity set at $I = 0.1$ or 10%, a more extensive range of turbulence intensities could be investigated to understand flow behaviour better.

3. **Optimization of DFSEM Parameters:** Investigate ideal DFSEM parameter settings, such as the spatial correlation function, eddy size distribution, and turbulence intensity, to improve the effectiveness of synthetic turbulence generation. Use optimization techniques to find parameter combinations that better agree with experimental results. Additionally, consider including FST data from prior simulations to offer more realistic inflow fluctuations. Furthermore, investigate using Reynolds stress data derived from experimental measurements to improve the accuracy and fidelity of turbulent flow predictions. This thesis was mainly based on internally generated Reynolds stress values, and including experimental data could

provide valuable insights into the performance of DFSEM in capturing actual turbulent flow characteristics.

By exploring these prospective research directions, it is possible to improve the understanding of turbulent flow phenomena and better computational tools for effectively forecasting and simulating complicated fluid dynamics scenarios. These activities help advance computational fluid dynamics methodology and engineering, science, and technology applications.

Bibliography

[1] Andrey Nikolaevich Kolmogorov. The local structure of turbulence in incompressible viscous fluid for very large reynolds. *Numbers. In Dokl. Akad. Nauk SSSR*, 30:301, 1941.

[2] Stewart Cant. Sb pope, turbulent flows, cambridge university press, cambridge, uk, 2000, 771 pp. *Combustion and Flame*, 125(4):1361–1362, 2001.

[3] Emmanuel Labourasse and Pierre Sagaut. Reconstruction of turbulent fluctuations using a hybrid rans/les approach. *Journal of computational Physics*, 182(1):301–336, 2002.

[4] Athony Leonard. Energy cascade in large-eddy simulations of turbulent fluid flows. In *Advances in geophysics*, volume 18, pages 237–248. Elsevier, 1975.

[5] Joep C Goeree, Geert H Keetels, Edwin A Munts, Hassan H Bugdayci, and Cees van Rhee. Concentration and velocity profiles of sediment-water mixtures using the drift flux model. *The Canadian Journal of Chemical Engineering*, 94(6):1048–1058, 2016.

[6] Raad I Issa. Solution of the implicitly discretised fluid flow equations by operator-splitting. *Journal of computational physics*, 62(1):40–65, 1986.

[7] VM Garcia-Alcaide, S Palleja-Cabre, R Castilla, Pedro Javier Gamez-Montero, J Romeu, T Pamies, Joan Amate, and Natalia Milán. Numerical study of the aerodynamics of sound sources in a bass-reflex port. *Engineering Applications of Computational Fluid Mechanics*, 11(1):210–224, 2017.

[8] A. Kandasamy B.N. Rajani and S. Majumdar. Numerical simulation of laminar flow past a circular cylinder. *Applied Mathematical Modelling*, 33(3):1228–1247, 2009.

[9] E. Berger and R. Wille. Periodic flow phenomena. *Annual Review of Fluid Mechanics*, 4:313–340, 1972.

[10] A. Roshko. On the drag and shedding frequency of two-dimensional bluff bodies. https://digital.library.unt.edu/ark:/67531/metadc57034/, 1954.

[11] C. Williamson. Oblique and parallel modes of vortex shedding in the wake of a circular cylinder at low reynolds numbers. *Journal of Fluid Mechanics*, 206:579–627, 1989.

[12] M. Braza, P. Chassaing, and H. Ha. Numerical study and physical analysis of the pressure and velocity field in the near wake of a circular cylinder. *Journal of Fluid Mechanics*, 165:79–130, 1986.

[13] I. Senocak and W. Shyy. A pressure-based method for turbulent cavitating flow computations. *J. Comput. Phys.*, 176(2):363–383, 2002.

[14] Rainer Friedrich and Michel Arnal. Analysing turbulent backward-facing step flow with the lowpass-filtered navier-stokes equations. *Journal of Wind Engineering and Industrial Aerodynamics*, 35:101–128, 1990.

[15] H-J Kaltenbach, M Fatica, R Mittal, TS Lund, and P Moin. Study of flow in a planar asymmetric diffuser using large-eddy simulation. *Journal of Fluid Mechanics*, 390:151–185, 1999.

[16] Michael Breuer and Wolfgang Rodi. Large-eddy simulation of turbulent flow through a straight square duct and a 180 bend. In *Direct and Large-Eddy Simulation I: Selected Papers from the First ERCOFTAC Workshop on Direct and Large-Eddy Simulation*, pages 273–285. Springer, 1994.

[17] Knut Akselvoll and Parviz Moin. Large-eddy simulation of turbulent confined coannular jets. *Journal of Fluid Mechanics*, 315:387–411, 1996.

[18] Thomas S Lund, Xiaohua Wu, and Kyle D Squires. Generation of turbulent inflow data for spatially-developing boundary layer simulations. *Journal of computational physics*, 140(2):233–258, 1998.

[19] Jean-Luc Aider and Alexandra Danet. Large-eddy simulation study of upstream boundary conditions influence upon a backward-facing step flow. *Comptes rendus. Mécanique*, 334(7):447–453, 2006.

[20] Meng Wang and Parviz Moin. Computation of trailing-edge flow and noise using large-eddy simulation. *AIAA journal*, 38(12):2201–2209, 2000.

[21] Pierre Sagaut, Eric Garnier, Eric Tromeur, Lionel Larcheveque, and Emmanuel Labourasse. Turbulent inflow conditions for large-eddy-simulation of compressible wall-bounded flows. *AIAA journal*, 42(3):469–477, 2004.

[22] A Ferrante and SE Elghobashi. A robust method for generating inflow conditions for direct simulations of spatially-developing turbulent boundary layers. *Journal of Computational Physics*, 198(1):372–387, 2004.

[23] Robert H Kraichnan. Diffusion by a random velocity field. *The physics of fluids*, 13(1):22–31, 1970.

[24] Robert Sugden Rogallo. *Numerical experiments in homogeneous turbulence*, volume 81315. National Aeronautics and Space Administration, 1981.

[25] Lars Davidson. Using isotropic synthetic fluctuations as inlet boundary conditions for unsteady simulations. *Advances and applications in Fluid Mechanics*, 1(1):1–35, 2007.

[26] Walid Bechara, Christophe Bailly, Philippe Lafon, and Sebastien M Candel. Stochastic approach to noise modeling for free turbulent flows. *AIAA journal*, 32(3):455–463, 1994.

[27] Markus Klein, Amsini Sadiki, and Johannes Janicka. A digital filter based generation of inflow data for spatially developing direct numerical or large eddy simulations. *Journal of computational Physics*, 186(2):652–665, 2003.

[28] Philipp Schlatter and Ramis Örlü. Turbulent boundary layers at moderate reynolds numbers: inflow length and tripping effects. *Journal of Fluid Mechanics*, 710:5–34, 2012.

[29] G Khujadze and Martin Oberlack. Dns and scaling laws from new symmetry groups of zpg turbulent boundary layer flow. *Theoretical and computational fluid dynamics*, 18:391–411, 2004.

[30] Nicolas Jarrin, Sofiane Benhamadouche, Dominique Laurence, and Robert Prosser. A synthetic-eddy-method for generating inflow conditions for large-eddy simulations. *International Journal of Heat and Fluid Flow*, 27(4):585–593, 2006.

[31] R Poletto, T Craft, and A Revell. A new divergence free synthetic eddy method for the reproduction of inlet flow conditions for les. *Flow, turbulence and combustion*, 91:519–539, 2013.

[32] Rui Wang and Zuoli Xiao. Influence of free-stream turbulence on the aerodynamic performance of a three-dimensional airfoil. *AIP Advances*, 11(7), 2021.

[33] Joseph Smagorinsky. General circulation experiments with the primitive equations: I. the basic experiment. *Monthly weather review*, 91(3):99–164, 1963.

[34] Akira Yoshizawa. Statistical theory for compressible turbulent shear flows, with the application to subgrid modeling. *The Physics of fluids*, 29(7):2152–2164, 1986.

[35] Elmar Achenbach. Experiments on the flow past spheres at very high reynolds numbers. *Journal of fluid mechanics*, 54(3):565–575, 1972.

[36] George Constantinescu and Kyle Squires. Numerical investigations of flow over a sphere in the subcritical and supercritical regimes. *Physics of fluids*, 16(5):1449–1466, 2004.

[37] Masaya Muto, Makoto Tsubokura, and Nobuyuki Oshima. Negative magnus lift on a rotating sphere at around the critical reynolds number. *Physics of Fluids*, 24(1), 2012.

[38] Elmar Achenbach. Vortex shedding from spheres. *Journal of Fluid Mechanics*, 62(2):209–221, 1974.